Developmental conversion of thymocyte-attracting cells into self-antigen-displaying cells in embryonic thymus medulla epithelium

Izumi Ohigashi[1], Andrea J. White[2], Mei-Ting Yang[3], Sayumi Fujimori[1], Yu Tanaka[3#], Alison Jacques[3], Hiroshi Kiyonari[4], Yosuke Matsushita[5], Sevilay Turan[6], Michael C. Kelly[7], Graham Anderson[2], Yousuke Takahama[3*]

[1]Division of Experimental Immunology, Institute of Advanced Medical Sciences, University of Tokushima, Tokushima 770-8503, Japan

[2]Institute for Immunology and Immunotherapy, University of Birmingham, Birmingham B15 2TT, UK

[3]Thymus Biology Section, Experimental Immunology Branch, National Cancer Institute, National Institutes of Health, Bethesda, Maryland 20892, USA

[4]Laboratory for Animal Resources and Genetic Engineering, RIKEN Center for Biosystems Dynamics Research, 2-2-3 Minatojima-minamimachi, Chuo, Kobe, Hyogo 650-0047, Japan

[5]Division of Genome Medicine, Institute of Advanced Medical Sciences, University of Tokushima, Tokushima 770-8503, Japan

[6]Sequencing Facility, Frederick National Laboratory for Cancer Research, National Cancer Institute, Frederick, MD 21701, USA

[7]Single Cell Analysis Facility, Cancer Research Technology Program, National Cancer Institute, National Institutes of Health, Bethesda, Maryland 20892, USA

[#]Present address; Department of Pediatrics, The University of Tokyo Hospital, 7-3-1 Hongo, Bunkyo, Tokyo 113-8655, Japan

[*]Corresponding author: <yousuke.takahama@nih.gov>

Abstract

Thymus medulla epithelium establishes immune self-tolerance and comprises diverse cellular subsets. Functionally relevant medullary thymic epithelial cells (mTECs) include a self-antigen-displaying subset that exhibits genome-wide promiscuous gene expression promoted by the nuclear protein Aire and that resembles a mosaic of extrathymic cells including mucosal tuft cells. An additional mTEC subset produces the chemokine CCL21, thereby attracting positively selected thymocytes from the cortex to the medulla. Both self-antigen-displaying and thymocyte-attracting mTEC subsets are essential for self-tolerance. Here we identify a developmental pathway by which mTECs gain their diversity in functionally distinct subsets. We show that CCL21-expressing mTECs arise early during thymus ontogeny. Fate-mapping analysis reveals that self-antigen-displaying mTECs, including Aire-expressing mTECs and thymic tuft cells, are derived from CCL21-expressing cells. The differentiation capability of CCL21-expressing embryonic mTECs is verified in reaggregate thymus experiments. These results indicate that CCL21-expressing embryonic mTECs carry a developmental potential to give rise to self-antigen-displaying mTECs, revealing that the sequential conversion of thymocyte-attracting subset into self-antigen-displaying subset serves to assemble functional diversity in the thymus medulla epithelium.

Running title: Functional conversion of embryonic mTECs

Introduction

The thymus medulla epithelium provides a unique environment for newly generated T cells to acquire self-tolerance before their emigration to the circulation. A variety of medullary thymic epithelial cells (mTECs) contribute to displaying self-antigens by employing multiple mechanisms. Promiscuous gene expression by a subpopulation of mTECs that express the nuclear protein Aire allows chromatin remodeling and genome-wide ectopic gene transcription[1,2]. Cellular mimesis in other mTEC subpopulations relies on a mosaic of tissue-specific transcription factor-dependent cells that individually resemble specialized cell types, including mucosal tuft cells and microfold cells[3,4]. These mTEC subpopulations form a self-antigen-displaying mTEC subset that provides various self-components, including extrathymic tissue-specific molecules, in the thymus medulla, so that newly generated T cells have an opportunity to establish central tolerance to genome-wide and systemic self-antigens prior to export from the thymus.

In addition to the self-antigen-displaying mTEC subset, there exists a medullary epithelial subset that produces the C-C chemokine CCL21, which attracts developing thymocytes and dendritic cells to the medullary region[5]. Positive selection-inducing TCR signals in newly generated cortical thymocytes elevate the expression of CCR7, a receptor for CCL21, and positively selected cortical thymocytes are therefore specifically attracted to migrate to the medullary region through the CCL21-CCR7-mediated chemotactic signals[6,7]. Two molecular species CCL21Ser and CCL21Leu with one amino acid difference are encoded in the mouse genome[8,9], and CCL21Ser encoded by *Ccl21a* locus is predominantly expressed in the thymus medulla[10]. In mice lacking either *Ccr7* or *Ccl21a*, positively selected mature thymocytes fail to accumulate in the medulla, and therefore T cells fail to establish self-tolerance[10-12]. Additional

CCR7-ligand CCL19 has no appreciable role in the cortex-to-medulla migration of developing thymocytes[10,13]. Thus, CCL21-expressing thymocyte-attracting mTECs represent a functional mTEC subset that is essential for the establishment of self-tolerance in T cells.

Aire-expressing mTECs primarily belong to MHC-II^{high} CD80^{high} mTEC subpopulation (mTEC^{high})[14,15], whereas most thymic mimetic cells are detectable in MHC-II^{low} CD80^{low} mTEC subpopulation (mTEC^{low}), which are derived from Aire-expressing mTEC^{high} cells[4,16-18]. The mTEC^{low} subpopulation is heterogeneous and contains immature mTEC progenitors that differentiate into the Aire-expressing mTEC^{high} subpopulation[19,20]. Consequently, the developmental progression of the self-antigen-displaying mTEC subset is considered to occur in the following sequence: mTEC^{low} progenitors -> mTEC^{high} Aire-expressing cells -> mTEC^{low} mimetic cells.

CCL21-expressing mTECs are mostly included in the mTEC^{low} subpopulation[21]. However, how the CCL21-expressing mTEC subset is integrated with, and/or potentially diverted from, the developmental progression of the self-antigen-displaying mTEC subset remains unknown. A single cell RNA-sequencing-based cluster analysis reported that *Ccl21a* transcripts are detectable within a heterogeneous “intertypical” TEC subpopulation, which includes cells with gene expression profiles resembling immature mTEC progenitors[22]. A more recent study has indicated that postnatally appearing mTEC-biased progenitors include cells that transcribe *Ccl21a*[23]. However, an independent single cell RNA-sequencing-based study suggested that TECs expressing *Ccl21a* transcripts represent a terminal population derived from “transit-amplifying” mTEC progenitors, by branching out of the self-antigen-displaying mTEC lineage[24]. Without the direct evaluation of developmental potential, it remains controversial and

unknown how CCL21-expressing mTECs are developmentally related to immature mTEC progenitors. It is even unclear how the *Ccl21a*-transcript-detectable TECs reported in these single cell transcriptomic studies are related to functionally relevant CCL21-protein-producing medullary TECs. More specifically, it remains unestablished whether the functionally relevant CCL21-expressing mTEC subset retains a developmental potential to give rise to the self-antigen-displaying mTEC subset.

The present study addresses whether the CCL21-expressing mTEC subset carries a developmental capability to differentiate into the self-antigen-displaying mTEC subset. We show that CCL21-expressing mTECs arise early during embryonic development in mice. By Cre-loxP-mediated fate-mapping analysis, we demonstrate that a vast majority of self-antigen-displaying mTEC subset, including Aire-expressing mTECs and thymic tuft cells, originates from CCL21-expressing cells. The developmental potential of CCL21-expressing embryonic mTECs to give rise to Aire-expressing mTECs is confirmed in reaggregate thymus experiments. These results indicate that functionally relevant CCL21-expressing mTEC subset contains a developmental capability to differentiate into self-antigen-displaying mTEC subset and that developmental conversion from thymocyte-attracting subset to self-antigen-displaying subset serves to assemble functional diversity in thymus medulla epithelium.

Results

CCL21-expressing mTECs arise in embryonic thymus

We began this study by examining the appearance of CCL21-expressing mTECs during mouse ontogeny. To do so, we analyzed CCL21-expressing mTECs by detecting tandem dimer Tomato (tdTomato) fluorescence proteins in *Ccl21a-tdTomato* knock-in mice. In the postnatal thymus of 5-week-old *Ccl21a*$^{tdTomato/+}$ mice, CCL21-expressing cells were detected in keratin 14 (Krt14)-expressing medullary TECs (Fig. 1A) and not in Ly51-expressing cortical TECs (Fig. 1B). Flow cytometric analysis confirmed that Ccl21a$^{tdTomato+}$ cells in the thymus are predominantly confined in EpCAM^{+} Ly51^{-} UEA1^{+} mTECs (Fig. 1C, D). In accordance with the medullary localization of CCL21-expressing mTECs, thymic medulla was abundant in CCL21 proteins (Fig. 1E), which contribute to attracting CCR7-expressing positively selected thymocytes from the cortex[7,10]. Among mTECs, most CCL21-expressing mTECs were distinct from Aire-expressing mTECs and DCLK1^{+} thymic tuft cells (Fig. 1F). CCL21-expressing mTECs equally distributed throughout the medullary region and were enriched neither in the pericortical area, including the corticomedullary junction area, nor in the central area within the medulla (Fig. 1G, H, Fig. S1A).

Analysis of embryonic thymus showed that CCL21-expressing cells in the central region of the thymus were prominent by embryonic day 15 (E15) (Fig. 2A) and detectable as early as E13 (Fig. 2B). The localization of CCL21-expressing cells in the central region of embryonic thymus lobes and their expression of Krt14 and Foxn1 ascertained that CCL21-expressing embryonic thymus cells represented mTECs (Fig. 2A-C), rather than neighboring CCL21^{+} parathyroid gland cells (Fig. 2B), which contribute to the attraction of hematopoietic cells to the pre-vascularized embryonic thymus[25]. CCL21 proteins were detectable in the medullary region

proximal to Ccl21a^{tdTomato}-expressing mTECs in the embryonic thymus by E15 (Fig. 2D), indicating that Ccl21a^{tdTomato}-expressing E15 embryonic mTECs represent functionally relevant CCL21-expressing mTECs. On the other hand, CCL21-expressing mTECs in the embryonic thymus were largely distinct from Aire-expressing mTECs and DCLK1^{+} thymic tuft cells (Fig. 2E). Similar to the postnatal thymus, CCL21-expressing mTECs in the embryonic thymus distributed throughout the medullary region and were not enriched in the pericortical areas including the corticomedullary junctions (Fig. 2F, G, Fig. S1B). These results indicate that CCL21-expressing mTECs arise by E15 in the central region of the embryonic thymus.

Fate mapping of CCL21-expressing cells in thymus

To better understand whether CCL21-expressing mTECs have a developmental potential to give rise to the self-antigen-displaying mTEC subset, we engineered mice in which the P1 bacteriophage-derived *Cre* recombinase gene was knocked-in at *Ccl21a* locus (Fig. 3A). We bred *Ccl21a*$^{Cre/+}$ mice with mice that carried a ubiquitous CAG promoter-driven loxP-stop-loxP-EGFP (CAG-loxP-EGFP) transgene. In *Ccl21a*-Cre x CAG-loxP-EGFP mice, EGFP expression labeled cells that have transcribed *Ccl21a* previously and/or presently (Fig. 3A).

In the postnatal thymus of 3-week-old *Ccl21a*-Cre x CAG-loxP-EGFP mice, EGFP signals in the thymus distributed prominently in the medullary region (Fig. 3B). EGFP^{+} cells in the medulla were detected in Krt14^{+} mTECs (Fig. 3B), including Aire^{+} mTECs and DCLK1^{+} thymic tuft cells (Fig. 3C). Flow cytometric analysis of enzyme-digested thymus cells showed that EGFP^{+} cells in the thymus were detected exclusively in EpCAM^{+}CD45^{-} TECs and not in EpCAM^{-}CD45^{+} hematopoietic cells, including thymocytes and dendritic cells, or EpCAM^{-}

CD45$^-$ cells, including mesenchymal fibroblasts and endothelial cells (Fig. 3D, E). Within EpCAM$^+$CD45$^-$ TECs, approximately 95% of UEA1$^+$Ly51$^-$ mTECs were EGFP$^+$, indicating that a vast majority of mTECs were derived from cells that previously transcribed *Ccl21a* (Fig. 3F, G). Flow cytometric analysis also confirmed the detection of Aire$^+$ UEA1$^+$Ly51$^-$ cells and DCLK1$^+$ UEA1$^+$Ly51$^-$ cells in EpCAM$^+$CD45$^-$ EGFP$^+$ TECs (Fig. 3H). Thus, self-antigen-displaying mTECs, including Aire$^+$ mTECs and DCLK1$^+$ thymic tuft cells, which do not presently express CCL21 (Fig. 1F, 2E), originate from *Ccl21a*$^+$ progenitors.

In the quantitative RT-PCR analysis of *Cre*, *Ccl21a*, and other TEC-associated genes, such as *Aire, Tnfrsf11a*, and *Psmb11*, *Cre* was detected specifically in the *Ccl21a*-expressing mTEC^{low} subpopulation, which includes the majority of CCL21-expressing mTECs[21], and not in the *Psmb11*-expressing cTECs or the *Aire- and Tnfrsf11a*-expressing mTEC^{high} subpopulation (Fig. 4A). These results verify the lineage tracing potential of *Ccl21a*-Cre-expressing cells to differentiate into the mTEC^{high} subpopulation including Aire$^+$ mTECs.

In addition to mTECs, approximately 66% of UEA1$^-$Ly51$^+$ cTECs in the postnatal thymus were EGFP$^+$ in 3-week-old *Ccl21a*-Cre x CAG-loxP-EGFP mice (Fig. 3 F, G). Section analysis of the thymus verified the presence of EGFP$^+$ cells in the cortex (Fig. 3B). Because cTECs do not presently express *Ccl21a* transcripts[10] (also shown in Fig. 1B-D), these results indicate that approximately two-thirds of postnatal cTECs are derived from cells that previously transcribed *Ccl21a* (Fig. 3 F, G). To characterize cTECs that previously transcribed *Ccl21a* and those that did not, we isolated EGFP$^+$ and EGFP$^-$ cTECs from 2-week-old postnatal *Ccl21a*-Cre x CAG-loxP-EGFP mice (Fig. S2) and performed deep-sequencing transcriptomic analysis. The MA plot and the volcano plot of RNA-sequencing data demonstrated high similarity in gene

expression profiles between EGFP$^+$ and EGFP$^-$ cTECs among 20,230 genes detected (Fig. 4B, C), unlike the pronounced difference in global gene expression profiles between cTECs and mTECs (Fig. S3A, B). The genes that are relevant for T cell-inducing and positive selection-inducing functions in cTECs, including *Dll4*, *Il7*, *Cxcl12*, *Psmb11*, *Ctsl*, *Prss16*, *Cd83*, *H-2K*, *H-2D*, and *I-Aβ*, were similarly abundant in EGFP$^+$ and EGFP$^-$ cTECs (Fig. S3C). These results suggest that cTECs derived from cells that either do or do not transcribe *Ccl21a* are functionally comparable to promote the generation and positive selection of cortical thymocytes.

Only 14 genes, including *Ccl21a*, showed significantly higher expression in EGFP$^+$ cTECs than in EGFP$^-$ cTECs, whereas only one gene, the parathyroid hormone-encoding *Pth*, showed significantly lower expression in EGFP$^+$ cTECs than in EGFP$^-$ cTECs (Fig. 4C, Fig. S3D). All the 14 genes that showed significantly higher expression in EGFP$^+$ cTECs than in EGFP$^-$ cTECs represented genes that showed higher expression in mTECs than in cTECs, and their expression, including *Ccl21a* expression, was much higher in mTECs than in EGFP$^+$ cTECs (Fig. S3D). Interestingly, EGFP$^+$ cTECs distributed unequally within the thymic cortex and were detected more frequently in the perimedullary cortical region than in the central cortical region or the subcapsular region of the cortex (Fig. 4D, E, Fig. S1C). In contrast, Ly51$^+$ total cTECs did not show such an unequal distribution in the thymic cortex (Fig. S1D, E). Thus, the intrathymic proximity to the medullary region contributes to the previous expression of *Ccl21a* transcripts in cTECs, suggesting that approximately two-thirds of postnatal cTECs originate from *Ccl21a*$^+$ cells generated in the thymic medulla.

Collectively, these fate-mapping experiments demonstrate that a vast majority of mTECs, including the self-antigen-displaying mTEC subset, and approximately two-thirds of cTECs,

particularly cTECs in the perimedullary cortical region, are derived from progenitor cells that previously transcribed *Ccl21a*.

Ccl21a-expressing mTECs arise early in central region of thymus primordium

It is further interesting to note that EGFP$^+$ cells within Foxn1$^+$ mTECs were detected in the central region of the thymus primordium in *Ccl21a*-Cre x CAG-loxP-EGFP mice as early as E11 (Fig. 5A). The detection of EGFP$^+$ cells occurred earlier in the ontogeny than the detection of Ccl21a$^{tdTomato+}$ mTECs by E13 (Fig. 2B) and CCL21-protein-expressing mTECs by E15 (Fig. 2D). These sequential detections suggested that low-level *Ccl21a* transcription initiated as early as E11 during thymus organogenesis was sufficient to produce functional Cre proteins to mediate the expression of CAG-promoter-dependent EGFP proteins, but failed to produce a detectable amount of tdTomato or CCL21 proteins. Subsequent elevation of *Ccl21a* transcription level resulted in the production of detectable amounts of tdTomato proteins followed by CCL21 proteins. Indeed, single-cell RNA-sequencing analysis of *Ccl21a* transcript counts demonstrated that *Ccl21a* expression levels within individual *Epcam*$^+$ *Foxn1*$^+$ TECs elevated during the embryogenesis from E12 to E14 (Fig. 5B). At E14, *Ccl21a*^{low} cells were detected at an equivalent frequency in β5t$^+$ and β5t$^-$ TEC populations (Fig. 5B). *Ccl21a* transcription in CCL21-expressing mTECs was further elevated from embryonic to postnatal development, as shown by single-cell RNA-sequencing analysis of *Ccl21a* transcript counts (Fig. 5B) and verified by flow cytometric analysis of *Ccl21a*-dependent tdTomato expression levels (Fig. 5C). Importantly, *Ccl21a*$^+$ *Foxn1*$^+$ mTECs detected during early thymus organogenesis were localized in the central region of the thymus primordium and were anatomically and transcriptomically distinguishable from *Ccl21a*$^+$ *Gcm2*$^+$ parathyroid epithelial cells (Fig. 2B, 5A,

5D). These results reveal that *Ccl21a*$^{+}$ mTECs develop in the central region of the thymus primordium as early as E11 before the generation of detectably CCL21 protein-expressing mTECs in the embryonic thymus by E15.

CCL21-expressing mTECs are distinct from RANK-expressing mTECs

Along with the fate-mapping detection of the developmental potential in *Ccl21a*$^{+}$ cells, the early and temporal detection of *Ccl21a*$^{+}$ mTECs and CCL21-expressing mTECs during embryogenesis tempted us to speculate that *Ccl21a*$^{+}$ mTECs, and even CCL21-expressing mTECs, might possess mTEC progenitor activity. Previous studies reported that embryonic thymus develops RANK-expressing mTEC-restricted progenitors, which have a developmental capability to give rise to self-antigen-displaying mTECs, including Aire^{+} mTECs[26,27]. RANK-expressing mTEC progenitors arise in the thymus during embryogenesis downstream of mTEC stem cells, which originate from cTEC-trait-expressing bipotent progenitors[5,26-29]. We next examined whether CCL21-expressing mTECs might overlap with RANK-expressing mTEC progenitors in *CCL21*^{tdTomato} *RANK*^{Venus} embryonic thymus. Interestingly, however, we found that CCL21-expressing mTECs and RANK-expressing mTECs were largely distinct cell populations within the embryonic thymus (Fig. 6A, B), although they were closely localized within the medullary region (Fig. 6A). RNA-sequencing analysis of CCL21^{+}RANK^{-} and CCL21^{-}RANK^{+} TECs highly purified from *CCL21*^{tdTomato} *RANK*^{Venus} embryonic thymus (Fig. S4A) demonstrated that CCL21-expressing mTECs were markedly different from RANK-expressing mTECs in global gene expression profiles (Fig. 6C). Gene ontology enrichment analysis ascertained the difference in global gene expression profiles in CCL21-expressing mTECs and RANK-expressing mTECs (Fig. 6D). Indeed, CCL21-expressing mTECs retained

more cTEC-trait genes, including *Psmb11*, *Cxcl12*, *CD83*, and *Ackr4*, than RANK-expressing mTECs (Fig. 6E), suggesting that in comparison with RANK-expressing mTECs, CCL21-expressing mTECs are more recently derived from cTEC-trait-expressing bipotent TEC progenitors. However, similarly to RANK-expressing mTECs, CCL21-expressing mTECs expressed equivalent levels of some mTEC-trait transcripts, including *Krt5* and *Krt14* (Fig. 6E). Among the genes associated with TEC progenitor activity[30-35], *Trp63* and *Pax1* were predominant in CCL21-expressing mTECs, whereas *Plet1*, *Krt19*, *Cldn3*, *Cldn4*, and *Ly6a* were readily detectable in RANK-expressing mTECs (Fig. 6E). Thus, CCL21-expressing mTECs in embryonic thymus are largely distinct from RANK-expressing mTECs, whereas CCL21-expressing mTECs and RANK-expressing mTECs are proximally localized with each other within the thymus medulla.

Nonetheless, it is important to point out that fate-mapping experiments using *Ccl21a*-Cre x CAG-loxP-EGFP mice were unable to distinguish whether TEC progenitor activity resides in CCL21-expressing mTECs generated within the thymus or in CCL21-expressing non-mTECs including neighboring parathyroid cells.

Developmental potential of CCL21-expressing mTECs

To directly examine whether CCL21-expressing mTECs have a developmental potential to give rise to self-antigen-displaying mTECs, we finally traced the fate of CCL21-expressing mTECs within the thymus microenvironment. To do so, we employed reaggregate thymus organ culture experiments[36,37] where RelB-deficient thymic stromal cells do not generate any functional mTECs[38,39]. Reaggregate thymuses were transplanted under mouse kidney capsules for reconstitution with hematopoietic cells derived from recipient mice. In this experimental

condition, RelB-deficient thymic stromal cells were reaggregated with tdTomato-expressing mTECs highly purified from *Ccl21a*^{tdTomato} E17 embryos (Fig. S4B). Ccl21a$^{tdTomato+}$ mTECs had already become functional CCL21-protein-expressing mTECs by E17 (Fig. 2), and the accumulation of CD4^{+}CD8^{-} and CD4^{-}CD8^{+} thymocytes in E17 thymic medullary region was defective in mice deficient in CCL21 (Fig. 7A-C), so that the reaggregate thymus experiments would address whether functionally relevant CCL21-expressing mTECs give rise to other mTEC subpopulations including Aire^{+} mTECs.

We found that Ccl21a^{tdTomato}-positive EpCAM^{+}CD45^{-} mTECs isolated from *Ccl21a*$^{tdTomato/+}$ E17 embryos generated Aire^{+} Krt14^{+} mTECs in the thymus reaggregated with RelB-deficient thymic stromal cells (Fig. 8A). Aire^{+} Krt14^{+} mTECs also developed from an equal number of parallelly isolated *Ccl21a*^{tdTomato}-negative EpCAM^{+}CD45^{-} TECs (Fig. 8B), which included cTEC-mTEC bipotent TEC progenitors[5,23]. RelB-deficient thymic stromal reaggregates without additional TECs failed to generate Aire^{+} Krt14^{+} mTECs (Fig. 8C), whereas control organ culture using RelB-heterozygous thymus apparently developed medullary regions that contained Aire^{+} Krt14^{+} mTECs (Fig. 8D). Quantitative evaluation of Krt14^{+} medullary areas (Fig. 8E) within total thymus aggregates (Fig. 8F) demonstrated that *Ccl21a*$^{+}$ mTECs have a developmental potential to give rise to Aire^{+} Krt14^{+} mTECs, equivalently to and not statistically different from *Ccl21a*-negative TECs, including bipotent TEC progenitors (Fig. 8G, H). Interestingly, *Ccl21a*$^{+}$ mTECs were still detected in the Krt14^{+} medullary areas in reconstituted thymus reaggregated with either *Ccl21a*$^{+}$ mTECs or *Ccl21a*-negative TECs (Fig. 8I, J), indicating that *Ccl21a*$^{+}$ mTECs have a potential to maintain themselves in the thymus and that *Ccl21a*-negative TECs have a developmental potential to produce *Ccl21a*$^{+}$ mTECs. Most

importantly, these results directly indicate that functionally relevant CCL21-expressing mTECs have a developmental potential to give rise to Aire-expressing mTECs.

In contrast to CCL21-expressing mTECs isolated from E17 embryos, Ccl21a^{tdTomato}-positive EpCAM^{+}CD45^{-} mTECs isolated from 4-week-old *Ccl21a*$^{tdTomato/+}$ mice did not exhibit any signs of Aire^{+} Krt14^{+} mTEC generation in the thymus reaggregated with RelB-deficient thymic stromal cells (Fig. S5A-G), suggesting a decline in the developmental potential of CCL21^{+} mTECs during the ontogeny from embryonic to postnatal period. However, no detection of progeny could also result from technical caveats associated with reaggregate thymus organ culture conditions that were suitable for detection of the developmental potential of embryonic but not postnatal CCL21-expressing mTECs, or differences in the lifespan and/or turnover of embryonic and postnatal CCL21-expressing cells.

Throughout the development including E17 embryos, CCL21-expressing mTECs were localized specifically in the central region of the thymus and were Krt14^{+} (Fig. 1, 2, 6, 9A). However, single-cell RNA-sequencing analysis demonstrated that the global gene expression profiles were largely different between embryonic *Ccl21a*^{low} mTECs and 4-week-old postnatal *Ccl21a*^{high} mTECs (Fig. 9B). Indeed, the majority of CCL21-expressing mTECs at E17 but not the postnatal period simultaneously expressed cTEC-associated protein Ly51 and mTEC-associated UEA1-binding molecules on the cell surface (Fig. 9C). Ly51 expression was lower in embryonic TECs than postnatal TECs[40] and equivalently distributed in the thymus including the medullary region defined by Krt14-expressing mTECs centrally localized in E17 thymus (Fig. 9A). These results highlight the difference in molecular expression profiles, including Ly51 expression, between E17 CCL21-expressing mTECs and postnatal CCL21-expressing mTECs.

Discussion

The present results demonstrate that CCL21-expressing mTECs arise early during embryonic thymus development. *Ccl21a-Cre*-mediated detection reveals that *Ccl21a*$^+$ *Foxn1*$^+$ mTECs are detectable as early as E11 in the central region of the embryonic thymus, shortly after the organogenesis of the thymus primordium, and this is followed by the detection of *Ccl21a-tdTomato*-expressing mTECs by E13 and CCL21 protein-expressing mTECs by E15. *Ccl21a-Cre*-mediated fate-mapping analysis establishes that at 3 weeks old, a vast majority of mTECs, including the self-antigen-displaying mTECs such as Aire$^+$ mTECs and thymic tuft cells, and approximately two-thirds of cTECs originate from *Ccl21a*$^+$ cells. Most importantly, our results demonstrate that *Ccl21a-tdTomato*-expressing and functional CCL21 protein-producing mTECs isolated from E17 embryonic thymus have a developmental potential to give rise to the self-antigen-displaying mTECs in the thymus microenvironment. These results demonstrate a previously unknown process by which the diversity in the thymus medulla epithelium is generated during embryogenesis by the developmental conversion of the CCL21-expressing thymocyte-attracting mTEC subset into the self-antigen-displaying mTEC subset, including Aire-expressing mTECs and thymic tuft cells.

Functional conversion of the thymocyte-attracting mTEC subset into the self-antigen-displaying mTEC subset offers an interesting implication that the thymus medulla is formed by initially generating CCL21-expressing mTECs and attracting CCR7-expressing positively selected thymocytes from the cortex even before the subsequent display of self-antigens mediated by Aire+ mTECs and thymic mimetic cells. Failure to establish self-tolerance by the loss of *Ccr7* or *Ccl21a* in the thymus[10-12] underscored the importance of functional CCL21-expressing mTEC subset. Our present results showing developmental potential of functional

CCL21-expressing mTECs to give rise to self-antigen-displaying mTECs reveals an additionally important function of CCL21-expressing mTECs in forming the diversity in thymus medulla epithelium, including the self-antigen-displaying mTEC subset. Stepwise progression in mTEC development from thymocyte-attracting function to self-antigen-displaying function fits stepwise requirement to initially recruit newly generated T cells from the thymic cortex before tolerizing T cells to self-antigens. Down-regulation of CCL21 in functionally converted self-antigen-displaying mTECs may further contribute to the prevention of excessive negative selection of newly generated T cells to self-antigens.

Recent studies demonstrated that the function of the thymus medulla is not limited to the establishment of self-tolerance in conventional αβ T cells but extends to the development of innate lymphocytes, including invariant NKT cells and γδ T cells[41,42]. The developmental capability of CCL21-expressing mTECs may further extend to additional mTEC subpopulations that contribute to supporting the development of innate invariant lymphocytes. Thus, CCL21-expressing mTECs may represent a primordial mTECs which separate newly generated αβ T cells, γδ T cells and NKT cells from the thymic cortex to the medullary microenvironment for further selection and maturation.

In contrast to the robust generation of Aire$^+$ mTECs from embryonic CCL21$^+$ mTECs, our results show that the ability to give rise to Aire$^+$ mTECs was not detectable in postnatal CCL21$^+$ mTECs. The fact that no Aire$^+$ mTECs were detected in reaggregate thymus organ culture may reflect a postnatal decline in the developmental potential of CCL21$^+$ mTECs. However, it is also possible that the developmental kinetics and the requirements for postnatal CCL21$^+$ mTECs may be different from those for E17 CCL21$^+$ mTECs, so that the reaggregate

thymus organ culture conditions for detecting the development of E17 CCL21$^+$ mTECs may not be optimal for the detection of the survival and development of postnatal CCL21$^+$ mTECs.

Nevertheless, it is important to notice the difference in the developmental potential between embryonic and postnatal CCL21$^+$ mTECs in reaggregate thymus organ culture. Analysis of molecular expression profiles further highlighted the difference between embryonic and postnatal CCL21$^+$ mTECs. We think that CCL21$^+$ mTECs may be heterogenous in developmental capability. Embryonic CCL21$^+$ mTECs, which give rise to self-antigen-displaying mTECs including Aire$^+$ mTECs and mimetic mTECs, may also terminally differentiate into a subpopulation of CCL21$^+$ mTECs, which no longer have further developmental potential, and which represent the majority of postnatal CCL21$^+$ mTECs.

Interestingly, our results also reveal that approximately two-thirds of cTECs are derived from progenitor cells that previously transcribed *Ccl21a*. The previous expression of *Ccl21a* transcripts in the fraction of cTECs is influenced by the intrathymic proximity to the medullary region and is enriched in the perimedullary cortical region (Fig. 4E). Developmental capability to become cTECs is shown in *Ccl21a* gene-expressing cells, and it is unknown whether CCL21-protein-expressing functional mTECs retain the developmental potential to give rise to cTECs. In contrast, our results from reaggregate thymus experiments clarified that CCL21-protein-expressing functional mTECs have a developmental potential to convert into Aire-expressing mTECs. Consequently, we think that at least a fraction of *Ccl21a* transcript-expressing mTECs retain a bipotent developmental potential to give rise to both cTECs and mTECs. It is unclear whether most *Ccl21a*-expressing mTECs retain a bipotent developmental potential for cTECs and mTECs or *Ccl21a*-expressing mTECs represent a mixture of bipotent progenitors and lineage-committed mTEC progenitors. Because of the unequal distribution of EGFP-labeled

cTECs within the thymic cortex, initial signals to promote bipotent progenitors to mTEC lineage may be provided by molecules restricted in the central region of the embryonic thymus, and those signals may promote the transcription of *Ccl21a* at an early stage of mTECs, which still retain the potential to become cTECs. Further examination of cTEC potential, for example, by using CCL21-tdTomato-expressing cells that constitutively express GFP, may lead to a better understanding of the cTEC-generating capability in embryonic and postnatal CCL21^{+} mTECs. It is also interesting to examine whether GFP^{+} cTEC development in *Ccl21a*-Cre x CAG-loxP-EGFP mice is mediated through RelB-dependent mTEC developmental progression and/or dependent on developing thymocyte-dependent mTEC-nurturing 'crosstalk' signals.

Nusser, et al., recently identified two bipotent TEC progenitor populations: an early cTEC-biased progenitor population and a postnatal mTEC-biased progenitor population[23]. Interestingly, they noted that the postnatally appearing mTEC-biased progenitor population includes cells that transcribe *Ccl21a*[23]. It would be interesting to clarify whether and how those postnatal TEC progenitors overlap with the embryonic and postnatal CCL21-protein-expressing mTECs reported in this study. It would also be interesting to shed light on how differently *Ccl21a*$^{+}$ progenitors contribute to cTECs and mTECs over the ontogeny and whether the enrichment of *Ccl21a*$^{+}$ progenitor-derived cTECs in the perimedullary area reflects a temporal replacement of cTECs derived from *Ccl21a*$^{+}$ progenitors localized in the medulla.

Further characterization of CCL21-expressing mTECs carrying a developmental potential to give rise to self-antigen-displaying mTEC subset is of great interest. Our results highlight the difference between CCL21-expressing mTECs and previously characterized RANK-expressing mTEC-restricted progenitors. CCL21-expressing mTECs and RANK-expressing mTECs are detectable in E13 embryonic thymus, are proximally localized within the medullary region in the

thymus, and are capable of generating Aire-expressing mTECs. Unlike RANK-expressing mTECs, however, CCL21-expressing mTECs include developmental potential to give rise to cTECs. Gene expression profiles show that CCL21-expressing mTECs retained more cTEC-trait genes, including *Psmb11*, *Cxcl12*, *CD83*, and *Ackr4*, than RANK-expressing mTECs, suggesting that in comparison with RANK-expressing mTECs, CCL21-expressing mTECs are more closely related to and more recently derived from cTEC-trait-expressing bipotent TEC progenitors. Furthermore, it is interesting to note that recently described Krt19^{+} progenitors that give rise to multiple mature mTEC populations including Aire^{+} mTECs, mimetic mTECs, and postnatal CCL21^{+} mTECs, lack expression of CCL21 and RANK[33]. An important aspect of future work will be to examine whether CCL21-expressing mTECs, RANK-expressing mTECs and Krt19-expressing mTECs are linked in upstream-downstream relationships in a single developmental pathway, or are developmentally distinct and parallel progenitors to give rise to mTECs. Similarly, it will be interesting to better clarify possible heterogeneity in CCL21-expressing mTECs in relation to their ability to give rise to cTECs as well as mTECs. Nevertheless, the finding in our study that CCL21^{+} embryonic mTECs can give rise to Aire^{+} mTECs reveals a new source of an important component of the thymus medulla.

Our results show that 95% of mTECs are labeled with EGFP fluorescence and therefore derived from *Ccl21a*$^{+}$ progenitors, whereas 5% of mTECs are not labeled with EGFP fluorescence in *Ccl21a*-Cre x loxP-EGFP mice. Our previous study using β5t-driven Cre mice indicated fate-mapping of 95% EGFP^{+} mTECs in CAG-loxP-stop-loxP-EGFP-transgenic reporter mice used in this study and >99.5% ZsGreen^{+} mTECs in Rosa26-loxP-ZsGreen-knock-in reporter mice[43]. Consequently, we think that 95% EGFP^{+} cells in mTECs detected in this

study may indicate that virtually all (>99.5%) mTECs are derived from cells that once transcribed *Ccl21a*.

A previous study detected *Ccl21a* transcripts within a podoplanin-expressing TEC subpopulation that resembled immature TECs in postnatal thymus[44]. It was reported that podoplanin-expressing mTEC progenitors, also known as junctional TECs (jTECs), were localized at the corticomedullary junction[44]. However, our results show that CCL21-expressing mTECs in the embryonic and postnatal thymus distribute throughout the medullary region and are not enriched in the corticomedullary junctions (Fig. 1H, 2G). Indeed, the majority of CCL21-expressing mTECs in postnatal thymus did not express podoplanin (Fig. S5H). Moreover, podoplanin expression was broadly detected by the majority of embryonic E17 TECs, most of which were cTECs (Fig. S5H). Thus, neither podoplanin expression nor corticomedullary junctional distribution characterizes CCL21-expressing mTECs. More importantly, our results demonstrate developmental potential in thymocyte-attracting CCL21-expressing mTECs and identify developmental conversion between functionally distinct mTEC subsets, which serves to assemble a diverse medullary microenvironment in the thymus.

In conclusion, the present study establishes that CCL21-expressing functional mTEC subset carries a developmental potential to give rise to self-antigen-displaying mTECs, revealing that the sequential conversion of functionally distinct mTEC subsets from thymocyte-attracting cells into self-antigen-displaying cells contributes to the functional diversification of thymus medulla epithelium during embryonic development. The present results are likely to ignite many interesting questions, including the characterization of signals that drive the developmental conversion of mTECs and the elucidation of developmental pathways for diverse TEC subpopulations.

Materials and methods

Mice

C57BL/6 (B6) mice were obtained from The Jackson Laboratory (Bar Harbor, ME) and SLC (Shizuoka, Japan). Ccl21a-tdTomato knock-in mice[10], RelB-knockout mice[39], RANK-Venus transgenic mice[45], β5t-Venus knock-in mice[46], CAG-loxP-stop-loxP-EGFP transgenic mice[47], and Foxn1-GFP transgenic mice[48] were described previously. All mouse experiments were performed with consent from the Animal Experimentation Committee of the University of Tokushima (T2022–50), the Animal Care and Use Committee of the National Cancer Institute (ASP 21–431, ASP 21-432, and EIB-076–3), the Birmingham Animal Welfare and Ethical Review Board and UK Home Office Animal Licences (PP7518148 and PP2990911), and the Institutional Animal Care and Use Committee of RIKEN Kobe Branch (A2001-03).

Generation of Ccl21a-Cre mice

The targeting vector was prepared by subcloning *Ccl21a*-containing mouse genomic BAC fragments (Advanced GenoTechs) and Cre-encoding cDNA into a plasmid containing a pgk-neo cassette (Gene Bridges). The linearized targeting vector was introduced into TT2 ES cells[49]. Targeted knock-in alleles were screened by genomic PCR analysis and Southern blot analysis. The Ccl21a-Cre mice (https://large.riken.jp/distribution/mutant-list.html; Accession No. CDB1131K) are available to the scientific community and were backcrossed to B6 mouse strain for more than 5 generations. The knock-in allele is detected using PCR primers as follows; Cre-F, 5’-AGGTTCGTTCACTCATGGA-3’ and Cre-R, 5′-TCGACCAGTTTAGTTACCC-3′ (product size, 235bp). Wild-type allele is detected using PCR primers as follows; WT-F, 5′-

CTGGTCTCATCCTCAACTCA-3′ and WT-R, 5′-TGTAACCCTAGGATTGTAGG-3′ (product size, 1,563bp).

Reaggregate thymus experiments

Fetal thymus lobes isolated from relB-KO mice at embryonic day (E) 15 were organ cultured for 5 days on sponge-supported Nucleopore filters (Whatman) placed on Dulbecco's Modified Eagle Medium supplemented with 10% fetal bovine serum (FBS) and penicillin-streptomycin mixed solution. To eliminate endogenous hematopoietic cells from the lobes, 1.35 mM 2'-deoxyguanosine (dGuo) was added in the culture medium[36,37]. dGuo-treated thymus lobes were digested with 0.25% trypsin supplemented with 0.45 mM EDTA and 0.02% DNase I for 15 min at 37℃ and reaggregated with tdTomato^{+} or tdTomato^{-} TECs isolated from *Ccl21a*$^{\text{tdTomato/+}}$ mice at E17 or 4 weeks old. After one day culture on Nucleopore filters, reaggregated thymuses were transplanted under kidney capsules of B6 mice. dGuo-treated fetal thymus lobes isolated from RelB-deficient and RelB-heterozygous mice were also transplanted under kidney capsules of B6 mice. Grafts were harvested 5 weeks post transplantation.

Multicolor immunofluorescence analysis

Paraformaldehyde-fixed frozen tissues embedded in OCT compound (Sakura Finetek) were sliced into 10-μm-thick sections. The sections were stained with anti-CCL21 (Bio-Rad), anti-Aire (eBioscience), anti-Ly51 (Biolegend), anti-Krt14 (Biolegend), anti-DCLK1 (abcam), anti-CD4 (Biolegend), anti-CD8 (Biolegend) antibodies, anti-Foxn1 antiserum[50], and UEA-1 (Vector Laboratories). Images were analyzed with a TCS SP8 confocal laser scanning microscope (Leica).

Fluorescence distribution analysis

The plot profile intensity for the fluorescence image of each channel in the regions of interest (ROI) was measured using ImageJ software (https://imagej.nih.gov/ij/index.html). The fluorescence intensity at each horizontal distance with the total intensity of the vertically averaged tdTomato, EGFP, or Ly51 in the ROI was calculated as 100. The sum of tdTomato or EGFP intensities for the medullary region defined by Krt14 expression or UEA1 reactivity and for the cortical region was calculated.

Multicolor flow cytometric analysis and cell sorting

For the analysis of thymic epithelial cells (TECs), minced thymuses were digested with 0.5 unit/ml Liberase (Roche) in the presence of 0.02% DNase I (Roche). Single-cell suspensions were stained with antibodies specific for EpCAM (BioLegend), CD45 (eBioscience), Ly51 (Biolegend), Podoplanin (Biolegend), I-A^b (BioLegend), and for the reactivity with UEA-1 (Vector Laboratories). For the analysis of Aire and DCLK1, surface-stained cells were fixed in 5% formaldehyde neutral buffer solution (Nacarai Tesque), permeabilized in 1x permeabilization buffer (eBioscience), and stained with anti-Aire (eBioscience) or anti-DCLK1 (abcam) antibody. For the isolation of TECs, $CD45^-$ cells were enriched in magnetic bead conjugated anti-CD45 antibody (Miltenyi Biotec). Multicolor flow cytometry and cell sorting were performed on FACSVerse, FACSAria II, and LSRFortessa (BD Biosciences).

RNA-sequencing analysis

cDNAs were prepared by using SMART-Seq v4 Ultra Low Input RNA Kit, according to the manufacturer's protocol (Clontech). Sequencing libraries were generated by using a Nextera XT DNA Library Prep Kit, according to the manufacturer's protocol (Illumina). The concentration of libraries was measured by an ABI PRISM 7500 Real-time PCR system in combination with a Power SYBR Green PCR Master Mix (Thermo Fisher). Single-end sequencing of cDNA libraries with a read length of 51 was performed with HiSeq 1500 platform (Illumina). For RNA-sequencing analysis of CCL21^{+}RANK^{-} and CCL21^{-}RANK^{+} TECs isolated from *CCL21*^{tdTomato} *RANK*^{Venus} embryonic E17 thymus, RNA was prepared using Qiagen RNAeasy Plus Micro Kit with genomic DNA eliminator columns. RNA-sequencing samples were sequenced on NovaSeq_SP flowcell using Illumina TruSeq Stranded Total RNA Library Prep with 2x100bp paired-end sequencing. Data were analyzed by using CLC Genomics Workbench 12.0 (Qiagen) with default parameters.

Single cell RNA-sequencing analysis

E12 embryonic pharyngeal cells, E14 embryonic CD45^{-}EpCAM^{+} β5t-Venus^{+} and β5t-Venus^{-} TECs, E16 embryonic CD45^{-}EpCAM^{+} β5t-Venus^{+} and β5t-Venus^{-} TECs isolated from β5t-Venus knock-in mice, and 4-week-old postnatal TEC-enriched thymus cells were employed for single-cell RNA sequencing. 3′ mRNA-seq library was generated as outlined in the Chromium Connect platform using 3' v3.1 Single Cell RNA-Seq chemistry reagents from 10X Genomics. Reverse transcription and cDNA amplification were performed according to the manufacturer's instructions. Libraries were sequenced on NextSeq 2000 and FASTQ files were generated from demultiplexes raw base call files using Cell Ranger 6.1.1 mkfastq. Alignment, filtering, barcode counting, and UMI counting were performed using Cell Ranger 6.1.1 count with mouse

reference 3.0.0 (mm10 and Ensembl release 98). The resulting matrix was imported into Seurat (v4.3.0) in R v 4.3.0 to create a Seurat object. The object underwent normalization, filtering, scaling, and dimensionality reduction steps sequentially using Seurat build-in functions, with default parameters. To integrate all the filtered objects from each sample, the CCA algorithm was employed through the FindIntegrationAnchors and IntegrateData functions in Seurat. The Uniform Manifold Approximation and Projection (UMAP) plots were visualized using the DimPlot function of Seurat. The histograms were visualized using the ggplot2 package (v3.4.2).

Statistical analysis

Statistical significance was assessed using the two-tailed unpaired Student's t test with Welch's correction for unequal variances or one-way ANOVA with Tukey's correction.

Data availability

RNA sequencing data are deposited in The DNA Data Bank of Japan (https://www.ddbj.nig.ac.jp) BioProject database with the accession number PRJDB15439 and NCBI Gene Expression Omnibus (GEO) (https://www.ncbi.nlm.nih.gov/geo) database with the accession number GSE239913. Single-cell RNA-sequencing data are deposited in NCBI GEO with the accession number GSE243180.

Acknowledgments

We thank Drs. Takashi Amagai and Manami Itoi for providing anti-Foxn1 antibody, Dr. Thomas Boehm for providing Foxn1-GFP transgenic mice, Drs. Toyomasa Katagiri, Hitomi Kyuma, Eri Ootsu, Bao Tran, and Assiatu Crossman for technical assistance, and Drs. Alfred Singer, Richard Hodes, Mami Matsuda-Lennikov and Jie Li for reading the manuscript. This work was supported by the Intramural Research Program ZIA BC 011806 of the National Institutes of Health, the National Cancer Institute, and the Center for Cancer Research (Y.T.); by the JSPS KAKENHI 22K06900, the JSPS Bilateral Program 120219928, and the JST PRESTO Grant 22712940 (I.O.); and by the MRC Programme Grant MR/T029765/1 and the Wellcome Trust Collaborative Award SynThy 211944/Z/18/Z (G.A.).

References

1. Derbinski J, Schulte A, Kyewski B, Klein L. Promiscuous gene expression in medullary thymic epithelial cells mirrors the peripheral self. *Nat Immunol.* 2001 Nov;2(11):1032-9. doi: 10.1038/ni723.

2. Anderson MS, Venanzi ES, Klein L, Chen Z, Berzins SP, Turley SJ, von Boehmer H, Bronson R, Dierich A, Benoist C, Mathis D. Projection of an immunological self shadow within the thymus by the aire protein. *Science*. 2002 Nov 15;298(5597):1395-401. doi: 10.1126/science.1075958.

3. Farr AG, Dooley JL, Erickson M. Organization of thymic medullary epithelial heterogeneity: implications for mechanisms of epithelial differentiation. *Immunol Rev.* 2002 Nov;189:20-7. doi: 10.1034/j.1600-065x.2002.18903.x.

4. Michelson DA, Hase K, Kaisho T, Benoist C, Mathis D. Thymic epithelial cells co-opt lineage-defining transcription factors to eliminate autoreactive T cells. *Cell*. 2022 Jul 7;185(14):2542-2558.e18. doi: 10.1016/j.cell.2022.05.018.

5. Takahama Y, Ohigashi I, Baik S, Anderson G. Generation of diversity in thymic epithelial cells. *Nat Rev Immunol.* 2017 May;17(5):295-305. doi: 10.1038/nri.2017.12.

6. Ueno T, Saito F, Gray DH, Kuse S, Hieshima K, Nakano H, Kakiuchi T, Lipp M, Boyd RL, Takahama Y. CCR7 signals are essential for cortex-medulla migration of developing thymocytes. *J Exp Med.* 2004 Aug 16;200(4):493-505. doi: 10.1084/jem.20040643.

7. Takahama Y. Journey through the thymus: stromal guides for T-cell development and selection. *Nat Rev Immunol.* 2006 Feb;6(2):127-35. doi: 10.1038/nri1781.

8. Nakano H, Gunn MD. Gene duplications at the chemokine locus on mouse chromosome 4: multiple strain-specific haplotypes and the deletion of secondary lymphoid-organ chemokine and EBI-1 ligand chemokine genes in the plt mutation. *J Immunol.* 2001 Jan 1;166(1):361-9. doi: 10.4049/jimmunol.166.1.361.

9. Chen SC, Vassileva G, Kinsley D, Holzmann S, Manfra D, Wiekowski MT, Romani N, Lira SA. Ectopic expression of the murine chemokines CCL21a and CCL21b induces the formation of lymph node-like structures in pancreas, but not skin, of transgenic mice. *J Immunol.* 2002 Feb 1;168(3):1001-8. doi: 10.4049/jimmunol.168.3.1001.

10. Kozai M, Kubo Y, Katakai T, Kondo H, Kiyonari H, Schaeuble K, Luther SA, Ishimaru N, Ohigashi I, Takahama Y. Essential role of CCL21 in establishment of central self-tolerance in T cells. *J Exp Med.* 2017 Jul 3;214(7):1925-1935. doi: 10.1084/jem.20161864.

11. Kurobe H, Liu C, Ueno T, Saito F, Ohigashi I, Seach N, Arakaki R, Hayashi Y, Kitagawa T, Lipp M, Boyd RL, Takahama Y. CCR7-dependent cortex-to-medulla migration of positively selected thymocytes is essential for establishing central tolerance. *Immunity*. 2006 Feb;24(2):165-77. doi: 10.1016/j.immuni.2005.12.011.

12. Nitta T, Nitta S, Lei Y, Lipp M, Takahama Y. CCR7-mediated migration of developing thymocytes to the medulla is essential for negative selection to tissue-restricted antigens. *Proc Natl Acad Sci U S A.* 2009 Oct 6;106(40):17129-33. doi: 10.1073/pnas.0906956106.

13. Link A, Vogt TK, Favre S, Britschgi MR, Acha-Orbea H, Hinz B, Cyster JG, Luther SA. Fibroblastic reticular cells in lymph nodes regulate the homeostasis of naive T cells. *Nat Immunol.* 2007 Nov;8(11):1255-65. doi: 10.1038/ni1513.

14. Derbinski J, Gäbler J, Brors B, Tierling S, Jonnakuty S, Hergenhahn M, Peltonen L, Walter J, Kyewski B. Promiscuous gene expression in thymic epithelial cells is regulated at multiple levels. *J Exp Med.* 2005 Jul 4;202(1):33-45. doi: 10.1084/jem.20050471.

15. Gray DH, Seach N, Ueno T, Milton MK, Liston A, Lew AM, Goodnow CC, Boyd RL. Developmental kinetics, turnover, and stimulatory capacity of thymic epithelial cells. *Blood*. 2006 Dec 1;108(12):3777-85. doi: 10.1182/blood-2006-02-004531.

16. Miller CN, Proekt I, von Moltke J, Wells KL, Rajpurkar AR, Wang H, Rattay K, Khan IS, Metzger TC, Pollack JL, Fries AC, Lwin WW, Wigton EJ, Parent AV, Kyewski B, Erle DJ, Hogquist KA, Steinmetz LM, Locksley RM, Anderson MS. Thymic tuft cells promote an IL-4-enriched medulla and shape thymocyte development. *Nature*. 2018 Jul;559(7715):627-631. doi: 10.1038/s41586-018-0345-2.

17. Kadouri N, Nevo S, Goldfarb Y, Abramson J. Thymic epithelial cell heterogeneity: TEC by TEC. *Nat Rev Immunol.* 2020 Apr;20(4):239-253. doi: 10.1038/s41577-019-0238-0.

18. Metzger TC, Khan IS, Gardner JM, Mouchess ML, Johannes KP, Krawisz AK, Skrzypczynska KM, Anderson MS. Lineage tracing and cell ablation identify a post-Aire-expressing thymic epithelial cell population. *Cell Rep.* 2013 Oct 17;5(1):166-79. doi: 10.1016/j.celrep.2013.08.038.

19. Rossi SW, Kim MY, Leibbrandt A, Parnell SM, Jenkinson WE, Glanville SH, McConnell FM, Scott HS, Penninger JM, Jenkinson EJ, Lane PJ, Anderson G. RANK signals from $CD4^{+}3^{-}$ inducer cells regulate development of Aire-expressing epithelial cells in the thymic medulla. *J Exp Med.* 2007 Jun 11;204(6):1267-72. doi: 10.1084/jem.20062497.

20. Gäbler J, Arnold J, Kyewski B. Promiscuous gene expression and the developmental dynamics of medullary thymic epithelial cells. *Eur J Immunol.* 2007 Dec;37(12):3363-72. doi: 10.1002/eji.200737131.

21. Lkhagvasuren E, Sakata M, Ohigashi I, Takahama Y. Lymphotoxin β receptor regulates the development of CCL21-expressing subset of postnatal medullary thymic epithelial cells. *J Immunol.* 2013 May 15;190(10):5110-7. doi: 10.4049/jimmunol.1203203.

22. Baran-Gale J, Morgan MD, Maio S, Dhalla F, Calvo-Asensio I, Deadman ME, Handel AE, Maynard A, Chen S, Green F, Sit RV, Neff NF, Darmanis S, Tan W, May AP, Marioni JC, Ponting CP, Holländer GA. Ageing compromises mouse thymus function and remodels epithelial cell differentiation. *Elife*. 2020 Aug 25;9:e56221. doi: 10.7554/eLife.56221.

23. Nusser A, Sagar, Swann JB, Krauth B, Diekhoff D, Calderon L, Happe C, Grün D, Boehm T. Developmental dynamics of two bipotent thymic epithelial progenitor types. *Nature*. 2022 Jun;606(7912):165-171. doi: 10.1038/s41586-022-04752-8.

24. Wells KL, Miller CN, Gschwind AR, Wei W, Phipps JD, Anderson MS, Steinmetz LM. Combined transient ablation and single-cell RNA-sequencing reveals the development of medullary thymic epithelial cells. *Elife*. 2020 Nov 23;9:e60188. doi: 10.7554/eLife.60188.

25. Liu C, Saito F, Liu Z, Lei Y, Uehara S, Love P, Lipp M, Kondo S, Manley N, Takahama Y. Coordination between CCR7- and CCR9-mediated chemokine signals in prevascular fetal thymus colonization. *Blood*. 2006 Oct 15;108(8):2531-9. doi: 10.1182/blood-2006-05-024190.

26. Baik S, Sekai M, Hamazaki Y, Jenkinson WE, Anderson G. Relb acts downstream of medullary thymic epithelial stem cells and is essential for the emergence of $RANK^+$ medullary epithelial progenitors. *Eur J Immunol*. 2016 Apr;46(4):857-62. doi: 10.1002/eji.201546253.

27. Akiyama N, Takizawa N, Miyauchi M, Yanai H, Tateishi R, Shinzawa M, Yoshinaga R, Kurihara M, Demizu Y, Yasuda H, Yagi S, Wu G, Matsumoto M, Sakamoto R, Yoshida N, Penninger JM, Kobayashi Y, Inoue J, Akiyama T. Identification of embryonic precursor cells that differentiate into thymic epithelial cells expressing autoimmune regulator. *J Exp Med*. 2016 Jul 25;213(8):1441-58. doi: 10.1084/jem.20151780.

28. Sekai M, Hamazaki Y, Minato N. Medullary thymic epithelial stem cells maintain a functional thymus to ensure lifelong central T cell tolerance. *Immunity*. 2014 Nov 20;41(5):753-61. doi: 10.1016/j.immuni.2014.10.011.

29. Ohigashi I, Zuklys S, Sakata M, Mayer CE, Hamazaki Y, Minato N, Hollander GA, Takahama Y. Adult thymic medullary epithelium is maintained and regenerated by lineage-restricted cells rather than bipotent progenitors. *Cell Rep*. 2015 Nov 17;13(7):1432-1443. doi: 10.1016/j.celrep.2015.10.012.

30. Senoo M, Pinto F, Crum CP, McKeon F. p63 Is essential for the proliferative potential of stem cells in stratified epithelia. *Cell*. 2007 May 4;129(3):523-36. doi: 10.1016/j.cell.2007.02.045.

31. Wallin J, Eibel H, Neubüser A, Wilting J, Koseki H, Balling R. Pax1 is expressed during development of the thymus epithelium and is required for normal T-cell maturation. *Development*. 1996 Jan;122(1):23-30. doi: 10.1242/dev.122.1.23.

32. Ulyanchenko S, O'Neill KE, Medley T, Farley AM, Vaidya HJ, Cook AM, Blair NF, Blackburn CC. Identification of a bipotent epithelial progenitor population in the adult thymus. *Cell Rep*. 2016 Mar;14(12):2819-32. doi: 10.1016/j.celrep.2016.02.080.

33. Lucas B, White AJ, Klein F, Veiga-Villauriz C, Handel A, Bacon A, Cosway EJ, James KD, Parnell SM, Ohigashi I, Takahama Y, Jenkinson WE, Hollander GA, Lu WY, Anderson G. Embryonic keratin19+ progenitors generate multiple functionally distinct progeny to maintain epithelial diversity in the adult thymus medulla. *Nat Commun*. 2023 Apr;14(1):2066. doi: 10.1038/s41467-023-37589-4.

34. Hamazaki Y, Fujita H, Kobayashi T, Choi Y, Scott HS, Matsumoto M, Minato N. Medullary thymic epithelial cells expressing Aire represent a unique lineage derived from cells expressing claudin. *Nat Immunol.* 2007 Mar;8(3):304-11. doi: 10.1038/ni1438.

35. Wong K, Lister NL, Barsanti M, Lim JMC, Hammett MV, Khong DK, Siatskas C, Gray DHD, Boyd RL, Chidgey AP. Multilineage potential and self-renewal define an epithelial progenitor cell population in the adult thymus. *Cell Rep.* 2014 Aug;8(4):1198-209. doi: 10.1016/j.celrep.2014.07.029.

36. Anderson G, Jenkinson EJ, Moore NC, Owen JJ. MHC class II-positive epithelium and mesenchyme cells are both required for T-cell development in the thymus. *Nature*. 1993 Mar 4;362(6415):70-3. doi: 10.1038/362070a0.

37. White A, Jenkinson E, Anderson G. Reaggregate thymus cultures. *J Vis Exp.* 2008 Aug 28;(18):905. doi: 10.3791/905.

38. Weih F, Carrasco D, Durham SK, Barton DS, Rizzo CA, Ryseck RP, Lira SA, Bravo R. Multiorgan inflammation and hematopoietic abnormalities in mice with a targeted disruption of RelB, a member of the NF-kappa B/Rel family. *Cell.* 1995 Jan 27;80(2):331-40. doi: 10.1016/0092-8674(95)90416-6.

39. Burkly L, Hession C, Ogata L, Reilly C, Marconi LA, Olson D, Tizard R, Cate R, Lo D. Expression of relB is required for the development of thymic medulla and dendritic cells. *Nature*. 1995 Feb 9;373(6514):531-6. doi: 10.1038/373531a0.

40. Ripen AM, Nitta T, Murata S, Tanaka K, Takahama Y. Ontogeny of thymic cortical epithelial cells expressing the thymoproteasome subunit β5t. *Eur J Immunol*. 2011 May;41(5):1278-87. doi: 10.1002/eji.201041375.

41. White AJ, Jenkinson WE, Cowan JE, Parnell SM, Bacon A, Jones ND, Jenkinson EJ, Anderson G. An essential role for medullary thymic epithelial cells during the intrathymic development of invariant NKT cells. *J Immunol.* 2014 Mar 15;192(6):2659-66. doi: 10.4049/jimmunol.1303057.

42. Roberts NA, White AJ, Jenkinson WE, Turchinovich G, Nakamura K, Withers DR, McConnell FM, Desanti GE, Benezech C, Parnell SM, Cunningham AF, Paolino M, Penninger JM, Simon AK, Nitta T, Ohigashi I, Takahama Y, Caamano JH, Hayday AC, Lane PJ, Jenkinson EJ, Anderson G. Rank signaling links the development of invariant γδ T cell progenitors and Aire^{+} medullary epithelium. *Immunity*. 2012 Mar 23;36(3):427-37. doi: 10.1016/j.immuni.2012.01.016.

43. Ohigashi I, Zuklys S, Sakata M, Mayer CE, Zhanybekova S, Murata S, Tanaka K, Holländer GA, Takahama Y. Aire-expressing thymic medullary epithelial cells originate from β5t-expressing progenitor cells. *Proc Natl Acad Sci U S A.* 2013 Jun;110(24):9885-90. doi: 10.1073/pnas.1301799110.

44. Onder L, Nindl V, Scandella E, Chai Q, Cheng HW, Caviezel-Firner S, Novkovic M, Bomze D, Maier R, Mair F, Ledermann B, Becher B, Waisman A, Ludewig B. Alternative NF-κB signaling regulates mTEC differentiation from podoplanin-expressing precursors in the cortico-medullary junction. *Eur J Immunol.* 2015 Aug;45(8):2218-31. doi: 10.1002/eji.201545677.

45. McCarthy NI, Cowan JE, Nakamura K, Bacon A, Baik S, White AJ, Parnell SM, Jenkinson EJ, Jenkinson WE, Anderson G. Osteoprotegerin-mediated homeostasis of Rank+ thymic epithelial cells does not limit Foxp3+ regulatory T cell development. *J Immunol.* 2015 Sep;195(6)2675-82. doi: 10.4049/jimmunol.1501226.

46. Murata S, Sasaki K, Kishimoto T, Niwa S, Hayashi H, Takahama Y, Tanaka, K. Regulation of CD8+ T cell development by thymus-specific proteasomes. *Science.* 2007 Jun;316(5829):1337-53. doi: 10.1126/science.1141915

47. Kawamoto S, Niwa H, Tashiro F, Sano S, Kondoh G, Takeda J, Tabayashi K, Miyazaki J. A novel reporter mouse strain that expresses enhanced green fluorescent protein upon Cre-mediated recombination. *FEBS Lett* 2000 Mar;470(3):263-8. doi: 10.1016/s0014-5793(00)01338-7.

48. Terszowski G, Müller SM, Bleul CC, Blum C, Schirmbeck R, Reimann J, Pasquier LD, Amagai T, Boehm T, Rodewald HR. Evidence for a functional second thymus in mice. *Science.* 2006 Apr 14;312(5771):284-7. doi: 10.1126/science.1123497.

49. Yagi T, Tokunaga T, Furuta Y, Nada S, Yoshida M, Tsukada T, Saga Y, Takeda N, Ikawa Y, Aizawa S. A novel ES cell line, TT2, with high germline-differentiating potency. *Anal Biochem.* 1993 Oct; 214(1):70–76. 10.1006/abio.1993.1458

50. Itoi M, Tsukamoto N, Amagai T. Expression of Dll4 and CCL25 in Foxn1-negative epithelial cells in the post-natal thymus. *Int Immunol.* 2007 Feb;19(2):127–32. doi: 10.1093/intimm/dxl129.

Figure legends

Figure 1. CCL21-expressing mTECs in postnatal thymus.

(**A, B**) Immunofluorescence analysis of thymus sections from 5-week-old *Ccl21a*$^{tdTomato/+}$ mice. tdTomato fluorescence (white) was detected with Keratin 14 (Krt 14, red) (**A**) or Ly51 (green) (**B**). White lines indicate capsular outline of the thymus. Blue lines show cortico-medullary junction. Representative data from at least three independent experiments are shown. c, cortex. m, medulla. Scale bar, 200μm.

(**C**) Flow cytometric profiles of tdTomato fluorescence expression in EpCAM^{+}CD45^{-}UEA1^{+}Ly51^{-} mTECs (left) and EpCAM^{+}CD45^{-}UEA1^{-}Ly51^{+} cTECs (right) from *Ccl21a*$^{tdTomato/+}$ mice (black line histograms) and WT mice (gray shaded histograms). Numbers in histograms indicate frequency of cells within indicated area.

(**D**) Proportions (means and SEMs, n=3) of tdTomato^{+} cells in EpCAM^{+}CD45^{-}UEA1^{+}Ly51^{-} mTECs, EpCAM^{+}CD45^{-}UEA1^{-}Ly51^{+} cTECs, and EpCAM^{-} non-TECs analyzed as in **C**.

(**E, F**) Immunofluorescence analysis of thymus sections from 5-week-old *Ccl21a*$^{tdTomato/+}$ mice. tdTomato fluorescence (white) was detected with CCL21 (red) (**E**), Aire or DCLK1 (magenta) (**F**). White lines indicate capsular outline of the thymus. Blue lines show cortico-medullary junction. Representative data from at least three independent experiments are shown. c, cortex. m, medulla. Scale bar, 200μm (**E**) or 10μm (**F**).

(**G**) Distribution of tdTomato-expressing cells in the medullary region defined by Krt14 expression. Left panel shows representative tdTomato (red) and Krt14 (white) fluorescence signals in the thymus sections from *Ccl21a*$^{tdTomato/+}$ mice. Scale bar, 100μm. Right panel shows fluorescence intensity profiles of tdTomato (red line) and Krt14 (gray line) signals within the region of interest defined by dashed rectangles in the left panel. Medullary regions were equally divided into three areas into pericortical areas (PM) and central area (CM).

(**H**) tdTomato intensity (means and SEMs, n=3) in indicated areas (**G** and **Fig. S1A**) were calculated in comparison with total tdTomato intensity within the ROI. n.s., not significant.

Figure 2. CCL21-expressing mTECs in embryonic thymus.

(**A**) tdTomato fluorescence (white) detected in thymus sections from E15 *Ccl21a*$^{tdTomato/+}$ embryos. White lines indicate the capsular outline of the thymus. The image in central region identified by the box in upper panel is magnified in bottom panel. Representative data from at least three independent experiments are shown. Scale bar, 200μm.

(**B**) tdTomato (red) and GFP (green) fluorescence in thymus sections from E13 *Ccl21a*$^{tdTomato/+}$ x Foxn1-GFP-transgenic embryos (left). Dashed lines show the outlines for the thymus and parathyroid primordia. Central region of the thymus identified by the box in upper panel is magnified in bottom panel. Scale bar, 100μm. Right panel shows a representative flow cytometric profile for tdTomato and GFP in CD45^{-}EpCAM^{+} epithelial cells. Numbers in the contour plot indicate frequency of cells within indicated area.

(**C-E**) Immunofluorescence analysis of thymus sections from E15 *Ccl21a*$^{tdTomato/+}$ embryos. tdTomato fluorescence (white) was detected with Krt14 (red) (**C**), CCL21 (red) (**D**), Aire, or DCLK1 (magenta) (**E**). Blue lines show the cortico-medullary junction. Representative data from at least three independent experiments are shown. c, cortex. m, medulla. Scale bar, 10μm.

(**F**) Distribution of tdTomato-expressing cells in the medullary region defined by Krt14 expression. Left panel shows representative tdTomato (red) and Krt14 (white) fluorescence signals in the thymus sections from *Ccl21a*$^{tdTomato/+}$ E15 embryos. Scale bar, 100μm. Right panel shows fluorescence intensity profiles of tdTomato (red line) and Krt14 (gray line) signals within the region of interest defined by dashed rectangles in the left panel. The medullary regions were equally divided into three areas into pericortical areas (PM) and central area (CM).

(**G**) tdTomato intensity (means and SEMs, n=3) in indicated areas (**F** and **Fig. S1B**) were calculated in comparison with total tdTomato intensity within the ROI. n.s., not significant.

Figure 3. Fate mapping of *Ccl21a*-expressing cells in the thymus.

(**A**) Schematic illustration of Cre-dependent *Ccl21a*-specific EGFP expression in *Ccl21a*-Cre x CAG-loxP-stop-loxP-EGFP mice. FRT, flippase recognition target site. Neo, neomycin resistance gene. Arrows indicate PCR primers for allele genotyping.

(**B, C**) Immunofluorescence analysis of thymus sections from 3-week-old *Ccl21a*-Cre x CAG-loxP-EGFP mice. EGFP fluorescence (green) was detected with Krt14 (red) (**B**), Aire, or DCLK1 (magenta) (**C**). White lines indicate the capsular outline of the thymus. Blue lines show the cortico-medullary junction. Representative data from at least three independent experiments are shown. c, cortex. m, medulla. Scale bar, 200μm (**B**) or 10μm (**C**).

(**D**) Flow cytometric analysis of liberase-digested thymus cells isolated from 3-week-old *Ccl21a*-Cre x CAG-loxP-EGFP mice. Histograms show EGFP fluorescence expression in EpCAM^{+}CD45^{-} cells (left), EpCAM^{-}CD45^{+} cells (middle), and EpCAM^{-}CD45^{-} cells (right) prepared from *Ccl21a*-Cre x CAG-loxP-EGFP mice (black histograms) and littermate control (gray shaded histograms). Numbers in histograms indicate frequency of cells within indicated area.

(**E**) Proportions (means and SEMs, n=3) of EGFP^{+} cells in indicated cell populations analyzed as in **D**.

(**F**) Flow cytometric profiles of UEA1 reactivity and Ly51 expression in EpCAM^{+}CD45^{-} TECs (left). Histograms show EGFP fluorescence expression in EpCAM^{+}CD45^{-}UEA1^{+}Ly51^{-} mTECs (middle) and EpCAM^{+}CD45^{-}UEA1^{-}Ly51^{+} cTECs (right) from *Ccl21a*-Cre x CAG-loxP-EGFP mice (black histograms) and littermate control (gray shaded histograms). Numbers in the histograms indicate frequency of cells within indicated area.

(**G**) Proportions (means and SEMs, n=3) of EGFP$^+$ and EGFP$^-$ cells in EpCAM$^+$CD45$^-$UEA1$^+$Ly51$^-$ mTECs (left) and EpCAM$^+$CD45$^-$UEA1$^-$Ly51$^+$ cTECs (right) analyzed as in **F**.

(**H**) Flow cytometric analysis of liberase-digested thymus cells isolated from *Ccl21a*-Cre x CAG-loxP-EGFP mice at 3 weeks old. Contour plots show Aire (top), DCLK1 (bottom), or isotype control detection with UEA1 reactivity or Ly51 expression in EpCAM$^+$CD45$^-$ EGFP$^+$ TECs. Numbers in the plots indicate frequency of cells within the indicated area. Representative data from three independent experiments are shown.

Figure 4. Characterization of cTECs that previously transcribed *Ccl21a*.

(**A**) Quantitative RT-PCR analysis of *Cre* and indicated genes (means and SEMs, n=3) in cTECs (EpCAM$^+$CD45$^-$UEA1$^-$Ly51$^+$), mTEC^{low} (EpCAM$^+$CD45$^-$UEA1$^+$Ly51$^-$ I-A^{low}), and mTEC^{high} (EpCAM$^+$CD45$^-$UEA1$^+$Ly51$^-$ I-A^{high}) isolated from *Ccl21a*$^{Cre/+}$ mice.

(**B**) MA plot of 20,230 genes detected in RNA-sequencing analysis of EGFP$^+$ and EGFP$^-$ cTECs isolated from *Ccl21a*-Cre x CAG-loxP-EGFP mice at 2-week-old. Detected genes are plotted as log2 average total counts versus log2 fold changes (EGFP$^+$ cTECs/EGFP$^-$ cTECs).

(**C**) Volcano plot analysis of EGFP$^+$ and EGFP$^-$ cTECs. Detected genes are plotted as log2 fold changes (EGFP$^+$ cTECs/EGFP$^-$ cTECs) versus -log10 FDR p-values. Fourteen genes (red symbols) are more highly detected (log2 fold change > 1.7, FDR p-value < 0.05) in EGFP$^+$ cTECs than EGFP$^-$ cTECs, whereas one gene (blue symbol) is more highly detected (log2 fold change < -1.7, FDR p-value < 0.05) in EGFP$^-$ cTECs than EGFP$^+$ cTECs.

(**D**) Distribution of EGFP-expressing cells in the thymus. Left panel shows representative fluorescence signals for EGFP (green) in the thymus sections from *Ccl21a*-Cre x CAG-loxP-EGFP mice. The medullary region is defined by UEA1 reactivity (red). White lines indicate the capsular outline of the thymus. Blue lines show the cortico-medullary junction. Scale bar, 100μm. Right panel shows

fluorescence intensity profiles of EGFP (green line) and UEA1 (gray line) signals within the region of interest (ROI) defined by dashed rectangles in the left panel. Cortical regions were equally divided into three areas into subcapsular cortex (SC). central cortex, (CC), and perimedullary cortex (PC). M, medulla.

(**E**) EGFP intensity (means and SEMs, n=3) in indicated areas (**C** and **Fig. S1C**) were calculated in comparison with total EGFP intensity within the ROI. n.s., not significant.

Figure 5. *Ccl21a*-expressing mTECs during early thymus organogenesis.

(**A**) Immunofluorescence analysis of thymus section from *Ccl21a*-Cre x CAG-loxP-EGFP E11 embryos. EGFP (green) and Foxn1 (red) were analyzed as indicated. Dashed lines show the outline of the thymus and parathyroid primordia. Image in yellow box in the middle of the thymus is magnified in right panel. Scale bar, 100μm. Representative data from two independent experiments are shown.

(**B**) Single-cell RNA-sequencing analysis of *Epcam*$^{+}$*Foxn1*$^{+}$ TECs from E12, E14, and 4-week-old β5t-Venus knock-in mice. Normalized log transcript counts of *Ccl21a* mRNA (x-axis) and cell numbers (y-axis) are plotted. For E14 TECs, β5t-Venus^{+} and β5t-Venus^{-} TECs were sorted and analyzed in parallel. Numbers in histograms indicate frequency of cells within indicated area.

(**C**) Flow cytometric analysis of tdTomato expression in EpCAM^{+}CD45^{-} TECs isolated from E17 embryonic and 2-week-old postnatal *Ccl21a*$^{tdTomato/+}$ mice (black histograms) and WT mice (gray shaded histograms). Bottom plots indicate the proportions (means and SEMs, n=3) of tdTomato^{negative} (black), tdTomato^{medium} (blue), and tdTomato^{high} (magenta) cells within EpCAM^{+}CD45^{-} TECs as defined in top histograms.

(**D**) Single cell RNA-sequencing analysis of *Epcam*$^{+}$ E12 embryonic pharyngeal epithelial cells. Dots indicate UMAP plot of *Ccl21a*$^{+}$ *Foxn1*$^{+}$ mTECs (red), *Ccl21a*$^{+}$ *Gcm2*$^{+}$ parathyroid epithelial cells (green), and other cells (gray).

Figure 6. CCL21-expressing mTECs are distinct from RANK-expressing mTECs.

(**A**) Immunofluorescence analysis of tdTomato (red) and Venus (green) signals in thymus sections from *Ccl21a*$^{tdTomato/+}$ *RANK*^{Venus} mice at indicated embryonic age. White lines indicate the capsular outline of the thymus. Images in boxed regions in upper panels are magnified in bottom panels. Representative data from at least three independent experiments are shown.

(**B**) Flow cytometric profiles of tdTomato and Venus fluorescence signals in EpCAM^{+}CD45^{-} TECs isolated from *Ccl21a*^{tdTomato} *RANK*^{Venus} mice at indicated embryonic age.

(**C**) Principal component analysis of RNA-sequencing data of indicated cell populations isolated from *Ccl21a*$^{tdTomato/+}$ *RANK*^{Venus} E17 embryos.

(**D**) Enrichment analysis of ontology for genes that are differently expressed (RPKM > 1, fold change > 1.5 or < 1.5, FDR p-value < 0.05) between CCL21^{+}RANK^{-} and CCL21^{-}RANK^{+} TECs. Bars show the adjusted p-values of the top five categories enriched in CCL21^{+}RANK^{-} TECs (top) and CCL21^{-}RANK^{+} TECs (bottom). Numbers in parentheses indicate the number of categorized genes.

(**E**) RPKM values of indicated genes detected in RNA-sequencing analysis.

Figure 7. CCL21-expressing mTECs in E17 embryos are functional in thymocyte attraction.

(**A**) Immunofluorescence analysis of CD4, CD8, Krt14, and tdTomato in thymus sections from heterozygous (*Ccl21a*$^{tdTomato/+}$) control mice or homozygous (*Ccl21a* $^{tdTomato/tdTomato}$) CCL21-deficient mice at E17. E17 thymus sections were stained for CD4, CD8, and Krt14. Representative images for Krt14 (white), tdTomato fluorescence (red), and CD8 (green) expressions are shown. Blue lines indicate cortico-medullary junctions, according to the distribution of Krt14-expressing mTECs. tdTomato-positive cells were localized in the medullary regions. Scale bar, 50μm.

(**B**, **C**) Graphs show the means and SEMs (n = 3) of the numbers of CD4^{+}CD8^{-} (**B**) and CD4^{-}CD8^{+} (**C**) thymocytes per unit area (0.01 mm^{2}) in the medullary regions. **, P < 0.01; ***, P < 0.001.

Figure 8. Developmental potential of CCL21-expressing mTECs.

(**A**-**D**) Immunofluorescent staining of indicated thymus graft sections. Shown in upper panels are Krt14 expression (white). White lines indicate capsular outline of the thymus. Blue lines show Krt14^{+} medullary region. Scale bar, 500μm. Bottom panels show Krt14 (white) and Aire (magenta) fluorescence signals within yellow boxes in upper panels. Scale bar, 50μm. Grafts represent relB-KO thymic stroma reaggregated with tdTomato^{+} TECs (**A**) and tdTomato^{-} TECs (**B**) as well as fetal thymus lobe from RelB-KO mice (**C**) and RelB-heterozygous mice (**D**).

(**E**) Size of Krt14^{+} medullary areas (means and SEMs, n=6) in indicated thymus graft sections.

(**F**) Size of grafted thymus areas (means and SEMs, n=6) in indicated thymus graft sections.

(**G**) Proportion (means and SEMs, n=6) of Krt14^{+} medullary areas in the thymus areas in indicated thymus graft sections.

(**H**) Numbers of Aire^{+} mTECs per mm^{2} of Krt14^{+} medullary areas in indicated thymus graft sections.

(**I**) Immunofluorescence analysis of tdTomato (red) and Krt14 (white) in indicated thymus graft sections. Scale bar, 50μm.

(**J**) Numbers of tdTomato^{+} cells per mm^{2} of Krt14^{+} medullary areas in indicated thymus graft sections. All images are representative data from three independent experiments. *P<0.05, **P<0.01, ***P<0.001, n.s., not significant.

Figure 9. CCL21-expressing mTECs at E17 embryonic and postnatal period.

(**A**) Immunofluorescence analysis of thymus sections from E17 or 2-week-old *Ccl21a*$^{tdTomato/+}$ mice. tdTomato fluorescence (red) and Ly51 (green) expression are shown. White lines indicate thymic capsules. Blue lines indicate cortico-medullary junctions. Images in yellow boxes (top panels) are magnified in bottom panels. Representative data from at least three independent experiments are shown. c, cortex. m, medulla. Scale bar, 100μm.

(**B**) UMAP plots showing the clusters of *Ccl21a*$^{+}$ mTECs in single cell RNA-sequencing analysis of thymic epithelial cells isolated from E16 embryonic and 4-week-old postnatal mice. The majority of E16 *Ccl21a*$^{+}$ mTECs were *Ccl21a*^{low}, whereas the majority of postnatal *Ccl21a*$^{+}$ mTECs were *Ccl21a*^{high} (Fig. 5B, C).

(**C**) Flow cytometric profiles of UEA1 reactivity and Ly51 expression in tdTomato^{negative} EpCAM^{+}CD45^{-} TECs and tdTomato^{positive} EpCAM^{+}CD45^{-} TECs isolated from E17 embryonic and 2-week-old postnatal *Ccl21a*$^{tdTomato/+}$ mice. Numbers in the contour plots indicate frequency of cells within indicated area. Representative data from three independent experiments are shown.

Figure 1

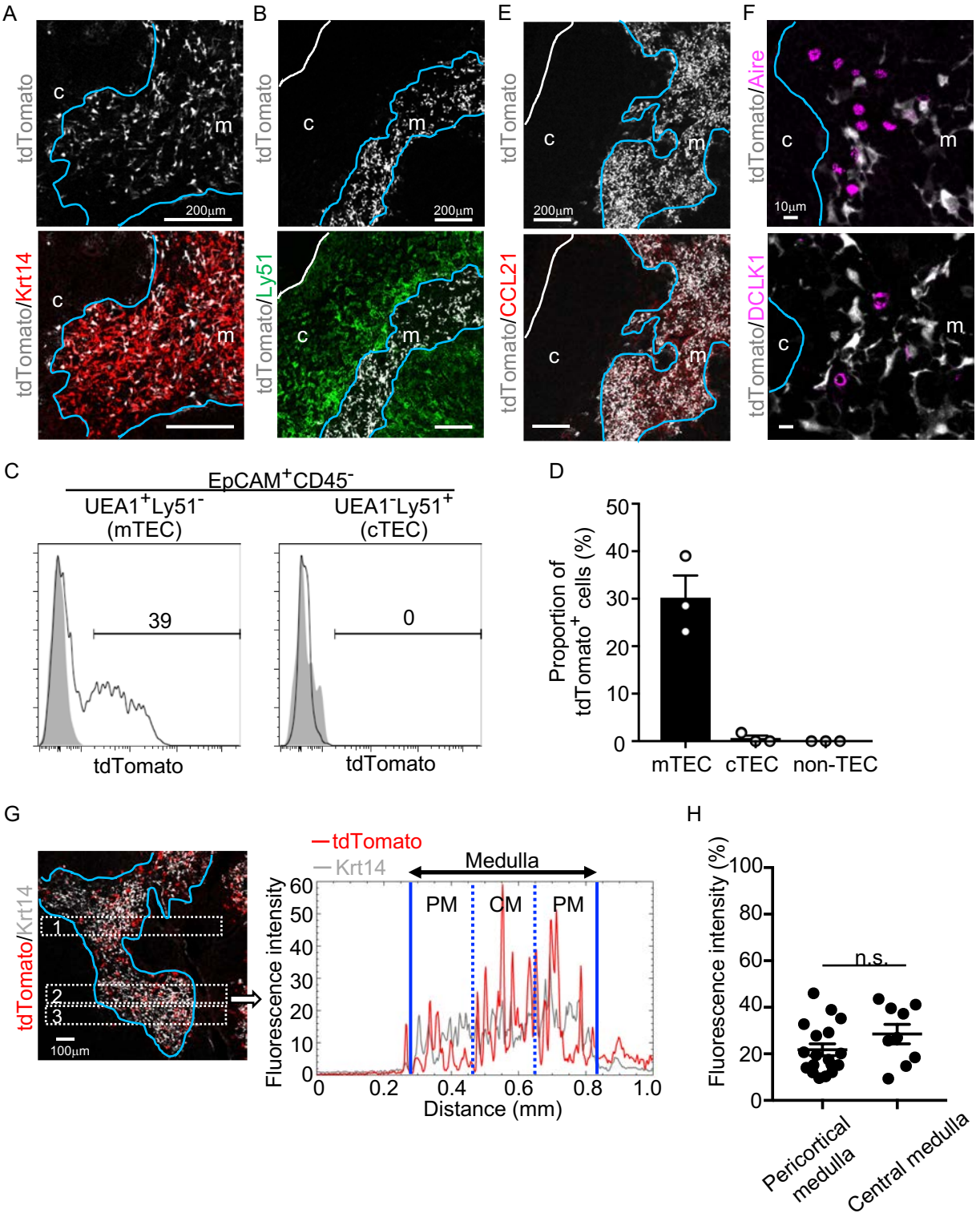
A
B
E
F
tdTomato
tdTomato/Krt14
tdTomato/Ly51
tdTomato/CCL21
tdTomato/Aire
tdTomato/DCLK1
c
m
200μm
10μm
C
EpCAM+CD45-
UEA1+Ly51-
(mTEC)
UEA1-Ly51+
(cTEC)
39
0
tdTomato
D
Proportion of
tdTomato+ cells (%)
50
40
30
20
10
0
mTEC
cTEC
non-TEC
G
tdTomato/Krt14
1
2
3
100μm
tdTomato
Krt14
Medulla
PM
CM
PM
Fluorescence intensity
Distance (mm)
0
0.2
0.4
0.6
0.8
1.0
H
Fluorescence intensity (%)
100
80
60
40
20
0
n.s.
Pericortical
medulla
Central medulla

Figure 2

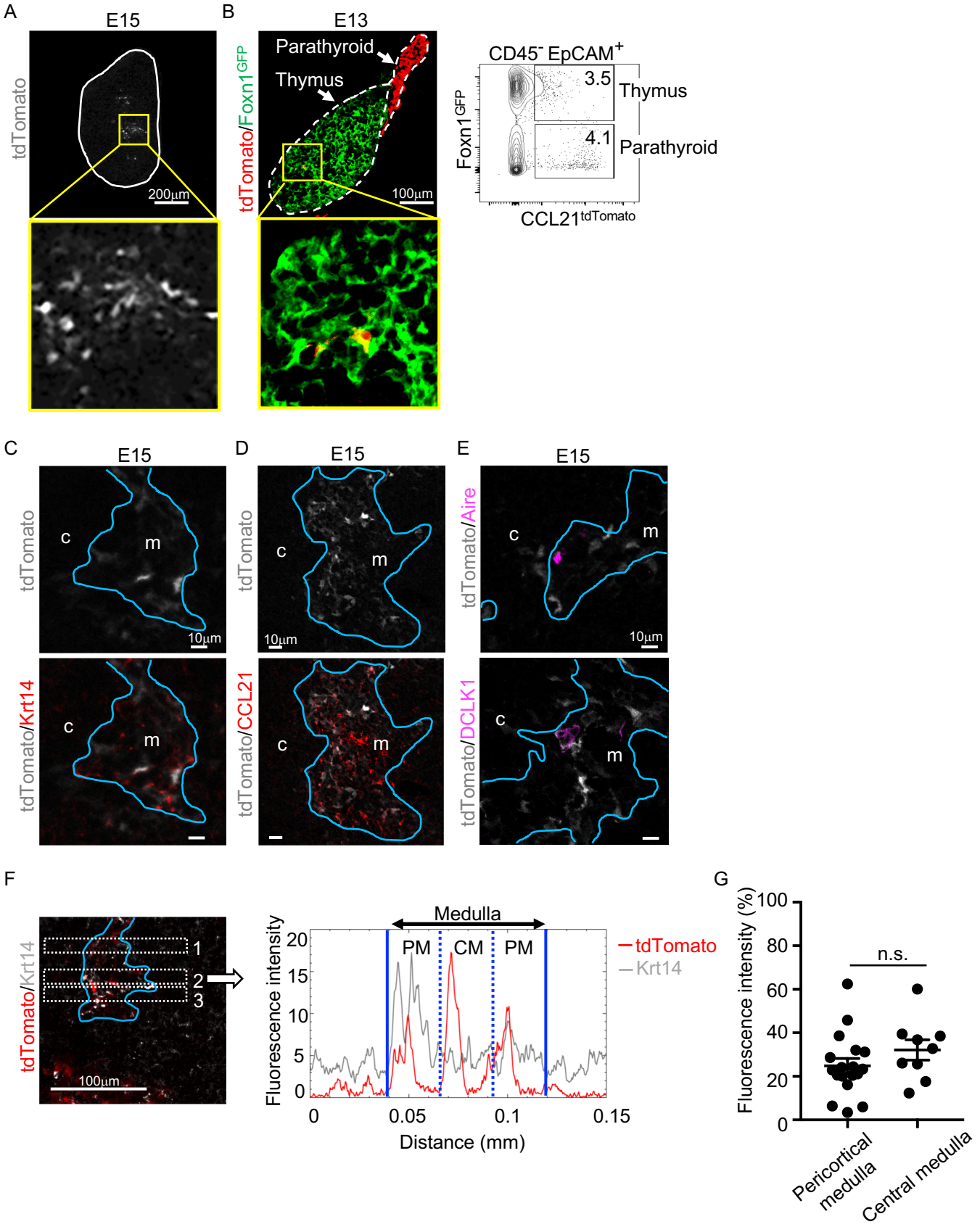
A
E15
tdTomato
200µm
B
E13
Parathyroid
Thymus
tdTomato/Foxn1GFP
100µm
CD45- EpCAM+
3.5
Thymus
4.1
Parathyroid
Foxn1GFP
CCL21tdTomato
C
E15
tdTomato
c
m
10µm
tdTomato/Krt14
D
E15
tdTomato/CCL21
E
E15
tdTomato/Aire
tdTomato/DCLK1
F
tdTomato/Krt14
1
2
3
100µm
Medulla
PM
CM
PM
tdTomato
Krt14
Fluorescence intensity
Distance (mm)
G
Fluorescence intensity (%)
n.s.
Pericortical medulla
Central medulla

Figure 3

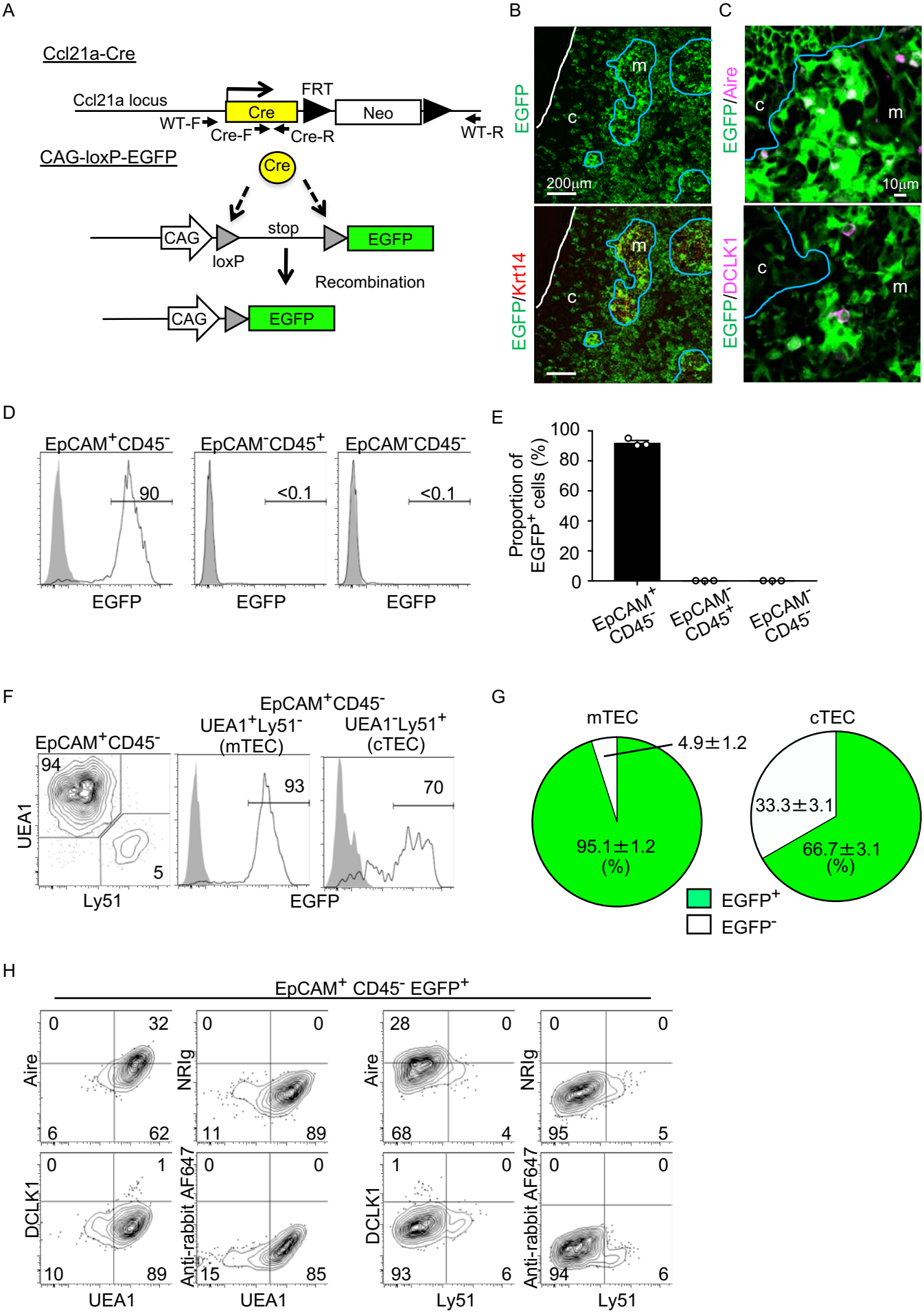
A
Ccl21a-Cre
Ccl21a locus
Cre
FRT
Neo
WT-F
Cre-F
Cre-R
WT-R
CAG-loxP-EGFP
Cre
CAG
stop
EGFP
loxP
Recombination
CAG
EGFP
B
EGFP
m
c
200μm
EGFP/Krt14
m
c
C
EGFP/Aire
c
m
10μm
EGFP/DCLK1
c
m
D
EpCAM+CD45-
90
EpCAM-CD45+
<0.1
EpCAM-CD45-
<0.1
EGFP
EGFP
EGFP
E
Proportion of EGFP+ cells (%)
100
80
60
40
20
0
EpCAM+ CD45-
EpCAM- CD45+
EpCAM- CD45-
F
EpCAM+CD45-
EpCAM+CD45-
UEA1+Ly51-
(mTEC)
UEA1-Ly51+
(cTEC)
94
5
93
70
UEA1
Ly51
EGFP
G
mTEC
4.9±1.2
95.1±1.2
(%)
cTEC
33.3±3.1
66.7±3.1
(%)
EGFP+
EGFP-
H
EpCAM+ CD45- EGFP+
Aire
NRIg
DCLK1
Anti-rabbit AF647
0
32
6
62
0
0
11
89
0
1
10
89
0
0
15
85
28
0
68
4
0
0
95
5
1
0
93
6
0
0
94
6
UEA1
UEA1
Ly51
Ly51

Figure 4

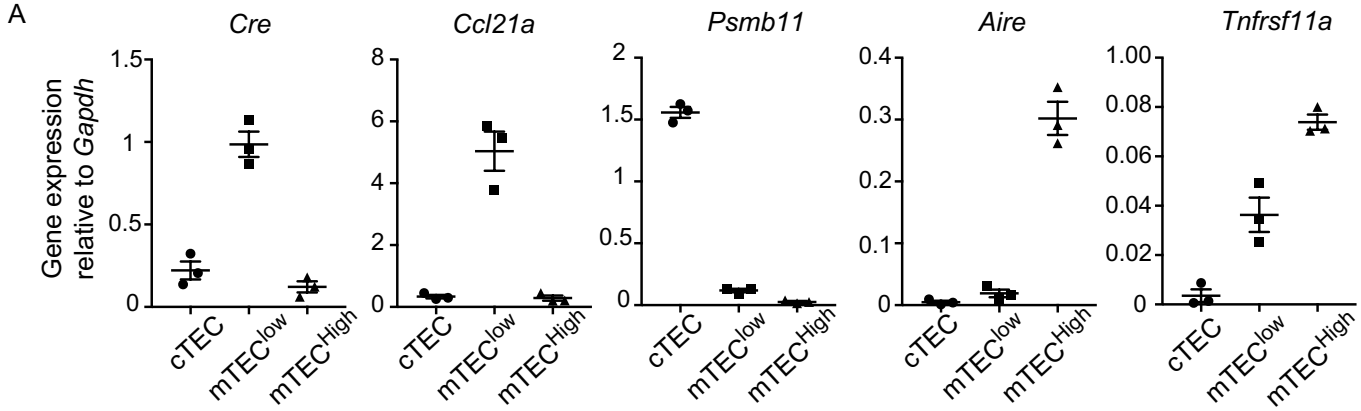
A
Cre
Ccl21a
Psmb11
Aire
Tnfrsf11a
Gene expression relative to Gapdh
cTEC
mTEC^low
mTEC^High

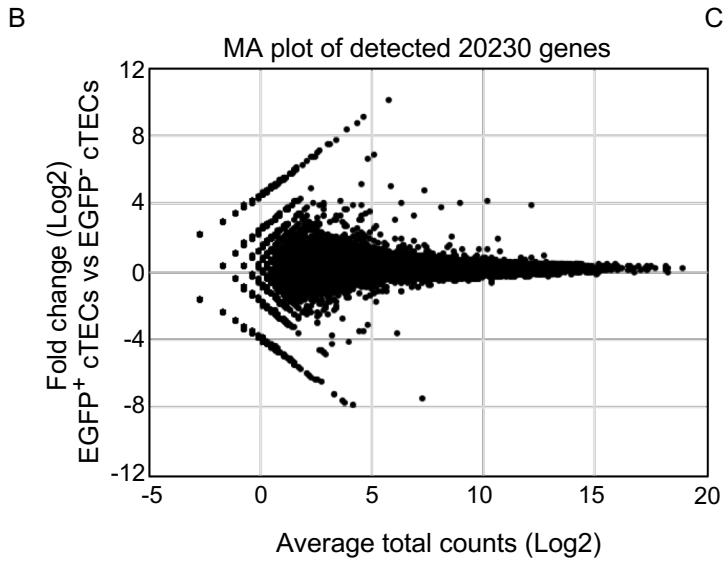
B
MA plot of detected 20230 genes
Fold change (Log2) EGFP+ cTECs vs EGFP- cTECs
Average total counts (Log2)

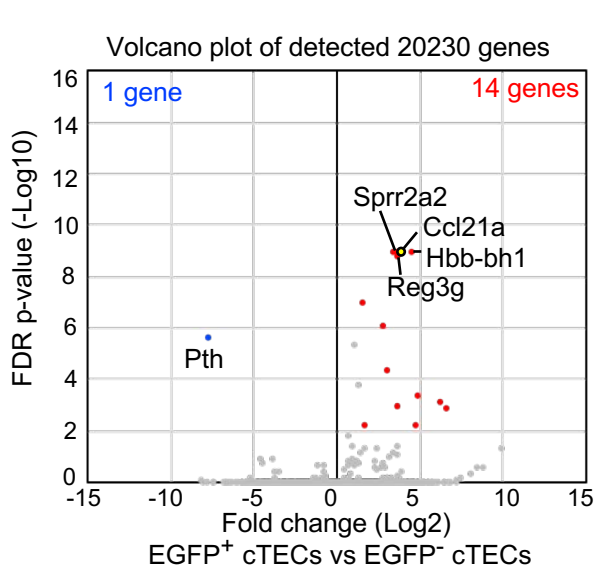
C
Volcano plot of detected 20230 genes
1 gene
14 genes
Sprr2a2
Ccl21a
Hbb-bh1
Reg3g
Pth
FDR p-value (-Log10)
Fold change (Log2) EGFP+ cTECs vs EGFP- cTECs

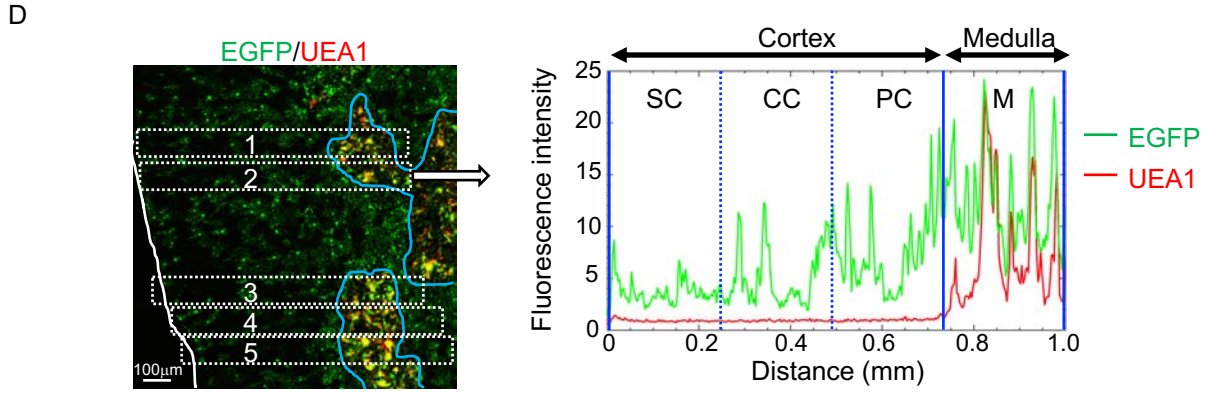
D
EGFP/UEA1
1
2
3
4
5
100μm
Cortex
Medulla
SC
CC
PC
M
EGFP
UEA1
Fluorescence intensity
Distance (mm)

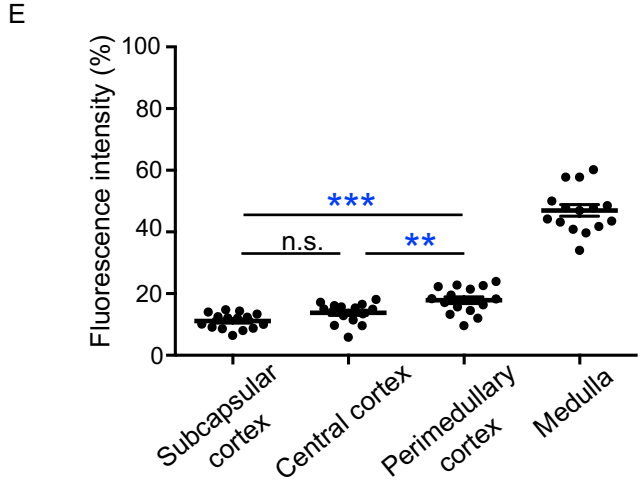
E
Fluorescence intensity (%)
***
n.s.
**
Subcapsular cortex
Central cortex
Perimedullary cortex
Medulla

Figure 5

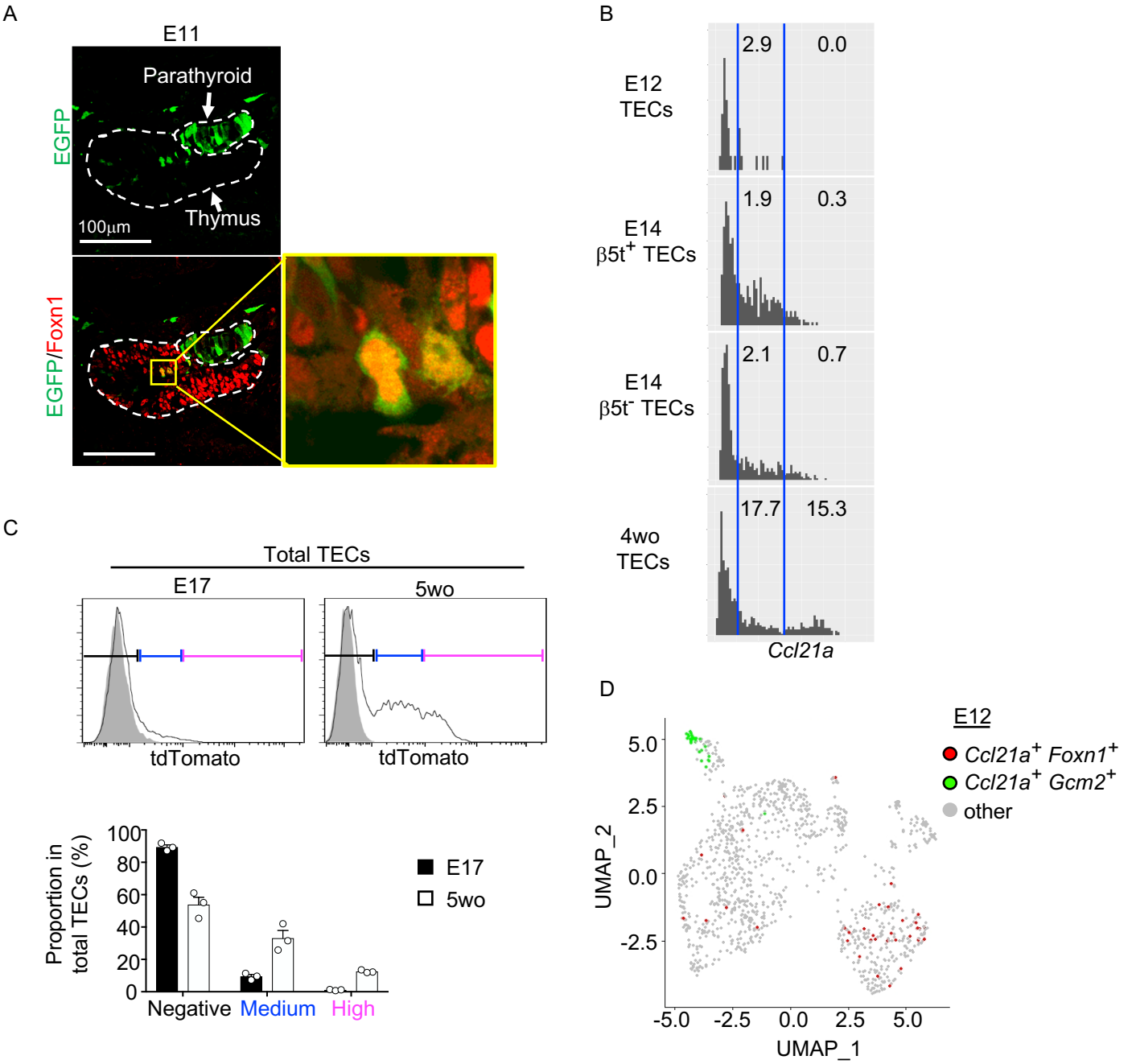
A
E11
Parathyroid
EGFP
Thymus
100μm
EGFP/Foxn1
B
E12
TECs
2.9
0.0
E14
β5t+ TECs
1.9
0.3
E14
β5t- TECs
2.1
0.7
4wo
TECs
17.7
15.3
Ccl21a
C
Total TECs
E17
5wo
tdTomato
tdTomato
Proportion in total TECs (%)
100
80
60
40
20
0
Negative
Medium
High
E17
5wo
D
E12
Ccl21a+ Foxn1+
Ccl21a+ Gcm2+
other
UMAP_2
5.0
2.5
0.0
-2.5
-5.0
-2.5
0.0
2.5
5.0
UMAP_1

Figure 6

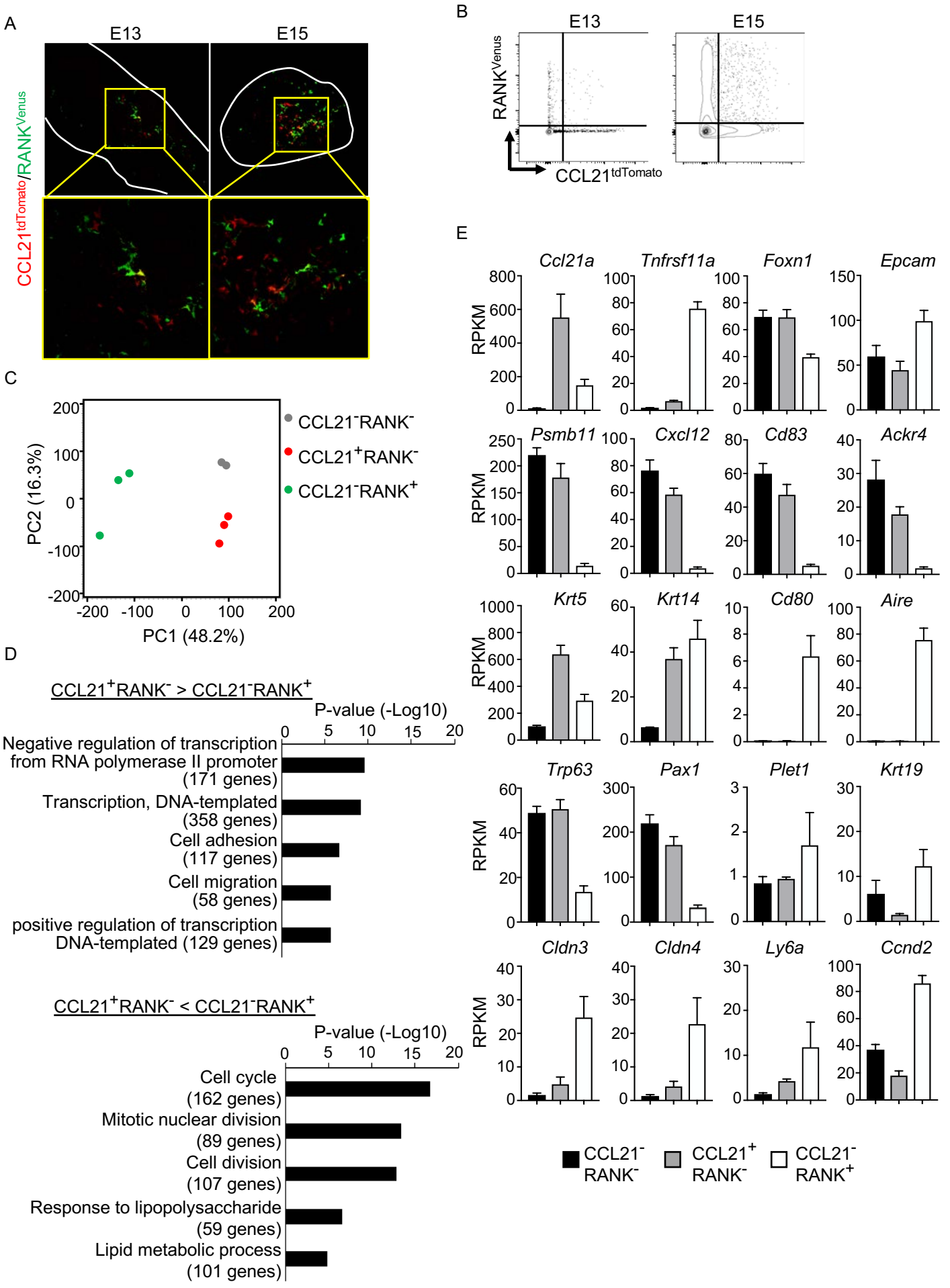
A
E13
E15
CCL21tdTomato/RANKVenus
B
E13
E15
RANKVenus
CCL21tdTomato
C
CCL21-RANK-
CCL21+RANK-
CCL21-RANK+
PC2 (16.3%)
PC1 (48.2%)
D
CCL21+RANK- > CCL21-RANK+
P-value (-Log10)
Negative regulation of transcription from RNA polymerase II promoter (171 genes)
Transcription, DNA-templated (358 genes)
Cell adhesion (117 genes)
Cell migration (58 genes)
positive regulation of transcription DNA-templated (129 genes)
CCL21+RANK- < CCL21-RANK+
P-value (-Log10)
Cell cycle (162 genes)
Mitotic nuclear division (89 genes)
Cell division (107 genes)
Response to lipopolysaccharide (59 genes)
Lipid metabolic process (101 genes)
E
Ccl21a
Tnfrsf11a
Foxn1
Epcam
Psmb11
Cxcl12
Cd83
Ackr4
Krt5
Krt14
Cd80
Aire
Trp63
Pax1
Plet1
Krt19
Cldn3
Cldn4
Ly6a
Ccnd2
RPKM
CCL21- RANK-
CCL21+ RANK-
CCL21- RANK+

Figure 7

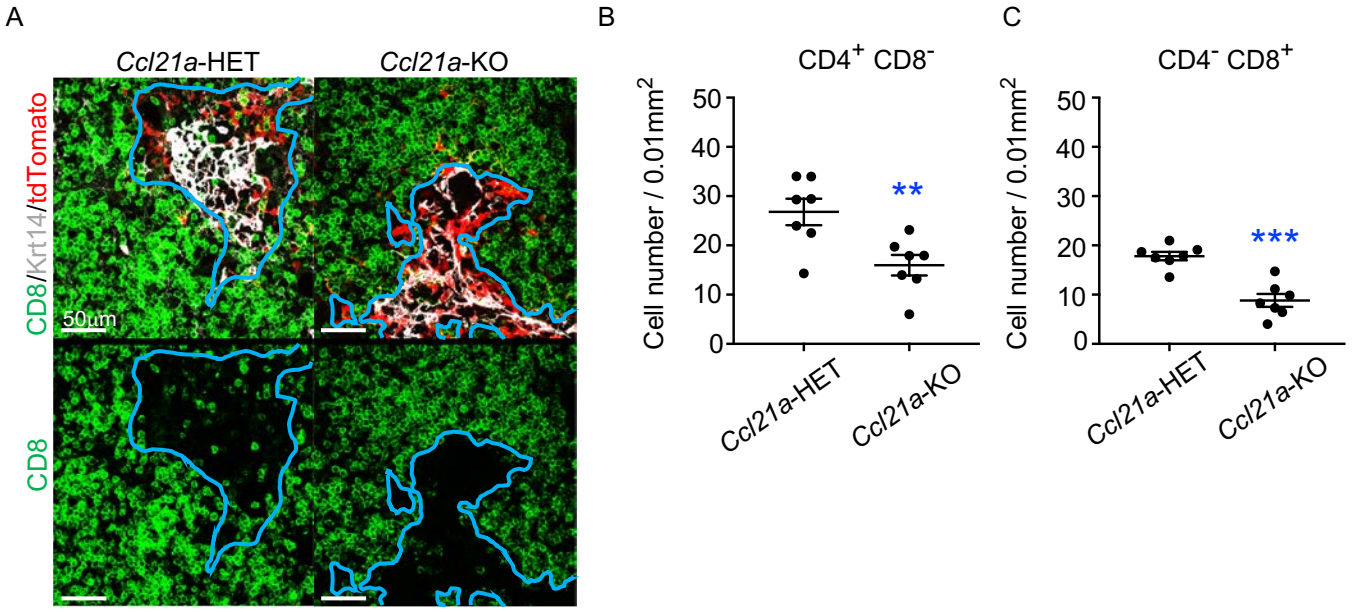
A
Ccl21a-HET
Ccl21a-KO
CD8/Krt14/tdTomato
CD8
50µm
B
CD4+ CD8-
Cell number / 0.01mm2
50
40
30
20
10
0
**
Ccl21a-HET
Ccl21a-KO
C
CD4- CD8+
Cell number / 0.01mm2
50
40
30
20
10
0
***
Ccl21a-HET
Ccl21a-KO

Figure 8

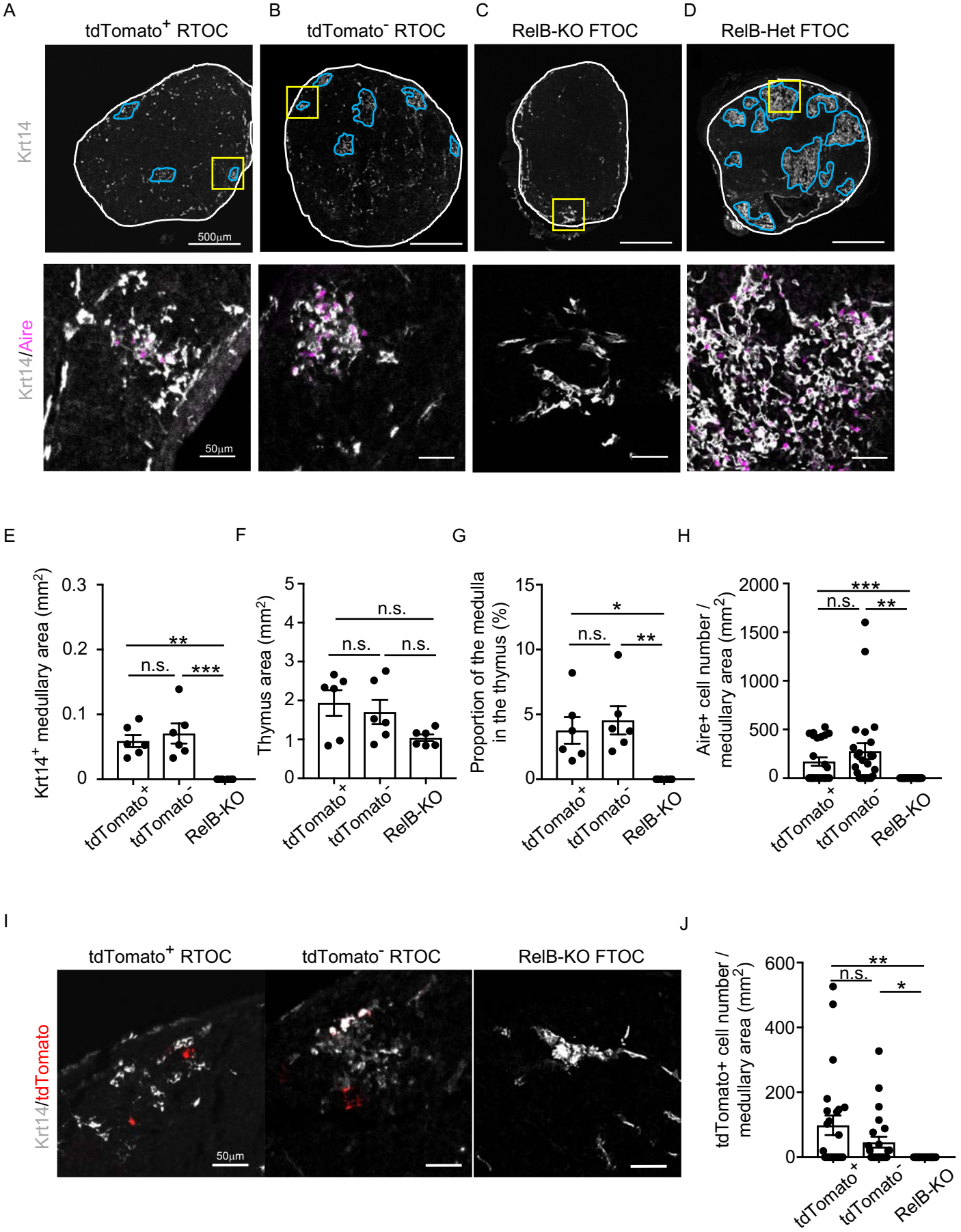
A
B
C
D
tdTomato+ RTOC
tdTomato- RTOC
RelB-KO FTOC
RelB-Het FTOC
Krt14
Krt14/Aire
500µm
50µm
E
F
G
H
Krt14+ medullary area (mm2)
Thymus area (mm2)
Proportion of the medulla in the thymus (%)
Aire+ cell number / medullary area (mm2)
n.s.
**
***
*
tdTomato+
tdTomato-
RelB-KO
I
J
Krt14/tdTomato
tdTomato+ cell number / medullary area (mm2)

Figure 9

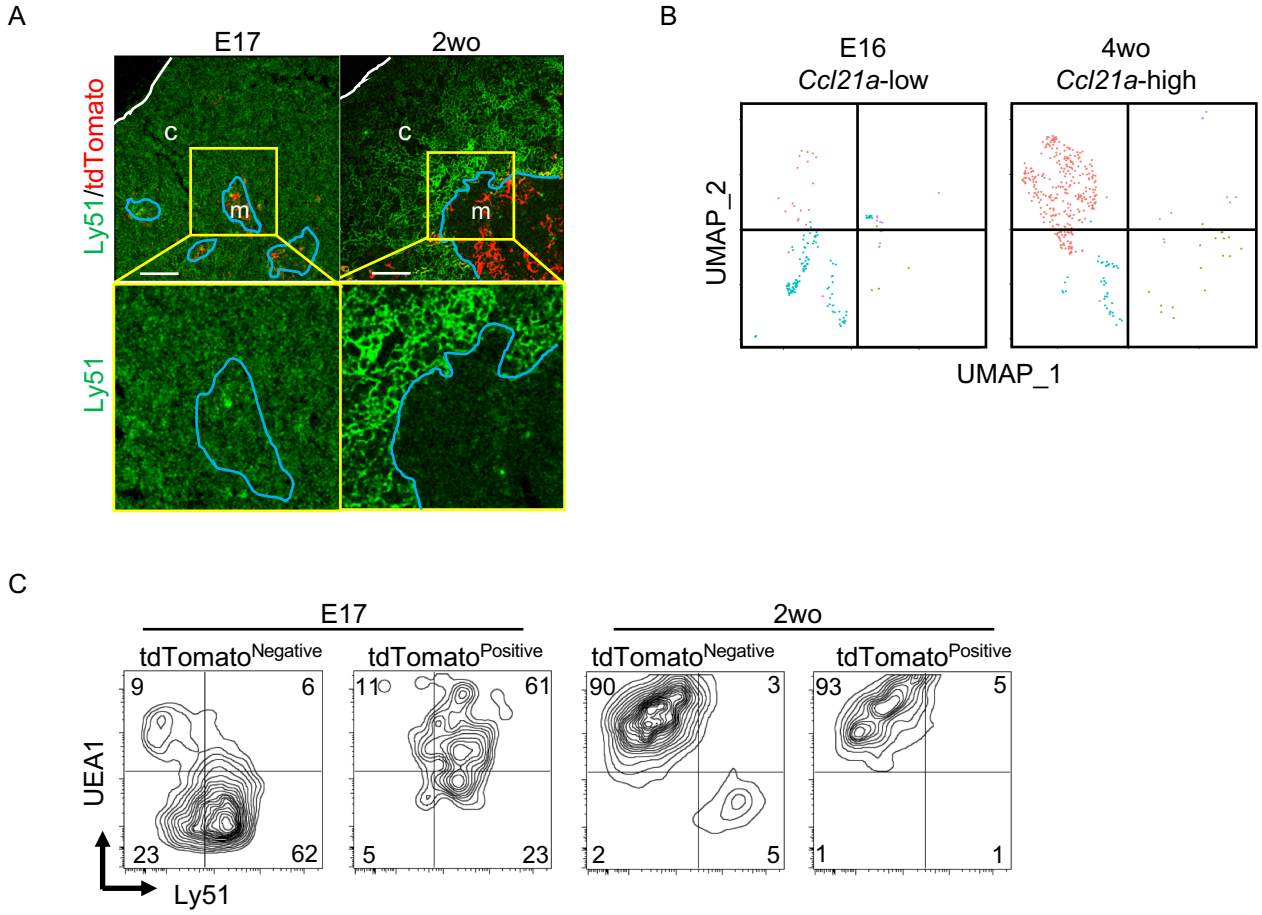
A
E17
2wo
Ly51/tdTomato
c
m
Ly51
B
E16
Ccl21a-low
4wo
Ccl21a-high
UMAP_2
UMAP_1
C
E17
2wo
tdTomato^Negative
tdTomato^Positive
tdTomato^Negative
tdTomato^Positive
UEA1
Ly51
9
6
23
62
11
61
5
23
90
3
2
5
93
5
1
1